1991-03

Determination of near-surface velocity fields in the CTZ using combined altimetric and inverse modelling techniques

Taggart, Douglas Michael

Monterey, California. Naval Postgraduate School

NAVAL POSTGRADUATE SCHOOL
Monterey, California

THESIS

DETERMINATION OF NEAR-SURFACE VELOCITY FIELDS IN THE CTZ USING COMBINED ALTIMETRIC AND INVERSE MODELLING TECHNIQUES

by

Douglas Michael Taggart

March 1991

Thesis Advisor — Steven R. Ramp
Co-Advisor — Newell Garfield

Approved for public release; distribution is unlimited

nclassified

curity classification of this page

REPORT DOCUMENTATION PAGE

a Report Security Classification Unclassified		1b Restrictive Markings	
a Security Classification Authority		3 Distribution Availability of Report	
b Declassification Downgrading Schedule		Approved for public release; distribution is unlimited.	
Performing Organization Report Number(s)		5 Monitoring Organization Report Number(s)	
a Name of Performing Organization Naval Postgraduate School	6b Office Symbol *(if applicable)* 35	7a Name of Monitoring Organization Naval Postgraduate School	
c Address *(city, state, and ZIP code)* Monterey, CA 93943-5000		7b Address *(city, state, and ZIP code)* Monterey, CA 93943-5000	
a Name of Funding Sponsoring Organization	8b Office Symbol *(if applicable)*	9 Procurement Instrument Identification Number	
c Address *(city, state, and ZIP code)*		10 Source of Funding Numbers	
		Program Element No	Project No / Task No / Work Unit Accession No

1 Title *(include security classification)* DETERMINATION OF NEAR-SURFACE VELOCITY FIELDS IN THE CTZ USING COMBINED ALTIMETRIC AND INVERSE MODELLING TECHNIQUES

2 Personal Author(s) Douglas Michael Taggart

3a Type of Report	13b Time Covered	14 Date of Report *(year, month, day)*	15 Page Count
Master's Thesis	From To	March 1991	54

6 Supplementary Notation The views expressed in this thesis are those of the author and do not reflect the official policy or position of the Department of Defense or the U.S. Government.

7 Cosati Codes			18 Subject Terms *(continue on reverse if necessary and identify by block number)*
ield	Group	Subgroup	inverse model,ocean currents,AVHRR,GEOSAT,radar altimeter

9 Abstract *(continue on reverse if necessary and identify by block number)*

An inverse model involving AVHRR imagery and the heat equation with dynamical constraints on the divergence, kinetic energy and vorticity of the solutions was used by Kelly (1989) to produce velocity fields that were in good agreement with Acoustic Doppler Current Profiler (ADCP) data. Dynamic heights derived from GEOSAT radar altimeter data have also been used to determine near-surface geostrophic currents. Synthetic GEOSAT-derived velocity data was generated from ADCP data collected as part of the Coastal Transition Zone (CTZ) Field Program. The inverse model was run with AVHRR imagery that was coincident to the CTZ Field Program ADCP data and the synthetic velocity data was added as an additional constraint on the model's solution. The resulting velocity solutions were much improved over those given by the inverse model alone. Refinement of this method involving a combination of different data sources should improve efforts to determine near-surface velocities of the ocean entirely by remote means.

0 Distribution Availability of Abstract	21 Abstract Security Classification	
☒ unclassified unlimited ☐ same as report ☐ DTIC users	Unclassified	
2a Name of Responsible Individual Steven R. Ramp	22b Telephone *(include Area code)* (408) 646-3162	22c Office Symbol OC/Ra

D FORM 1473,84 MAR 83 APR edition may be used until exhausted
All other editions are obsolete

security classification of this page

Unclassified

Approved for public release; distribution is unlimited.

Determination of Near-Surface Velocity Fields in the CTZ
Using Combined Altimetric and Inverse Modelling Techniques

by

Douglas Michael Taggart
Lieutenant Commander, United States Navy
B.S., United States Naval Academy, 1979

Submitted in partial fulfillment of the
requirements for the degree of

MASTER OF SCIENCE IN METEOROLOGY AND PHYSICAL OCEANOGRAPHY

from the

NAVAL POSTGRADUATE SCHOOL
March 1991

Curtis A. Collins, Chairman,
Department of Oceanography

ABSTRACT

An inverse model involving AVHRR imagery and the heat equation with dynamical constraints on the divergence, kinetic energy and vorticity of the solutions was used by Kelly (1989) to produce velocity fields that were in good agreement with Acoustic Doppler Current Profiler (ADCP) data. Dynamic heights derived from GEOSAT radar altimeter data have also been used to determine near-surface geostrophic currents. Synthetic GEOSAT-derived velocity data was generated from ADCP data collected as part of the Coastal Transition Zone (CTZ) Field Program. The inverse model was run with AVHRR imagery that was coincident to the CTZ Field Program ADCP data and the synthetic velocity data was added as an additional constraint on the model's solution. The resulting velocity solutions were much improved over those given by the inverse model alone. Refinement of this method involving a combination of different data sources should improve efforts to determine near-surface velocities of the ocean entirely by remote means.

TABLE OF CONTENTS

LIST OF TABLES

LIST OF FIGURES

ACKNOWLEDGEMENTS

I would like to thank Kathryn Kelly for the use of her model and the help and advice necessary for its successful use. I would also like to thank my advisor Steve Ramp and my coadvisor Toby Garfield for their assistance and guidance throughout the course of my thesis work. Yes, one of these days I will actually leave NPS to go to my next command! Rob Wyland provided the "eyes" for this project by helping with the manipulation of the imagery on the NPS IDEA lab. Arlene Bird provided the indispensible link to GTHESIS after I left NPS (more than once) with revisions still left to do. Last but not least; I owe too much to my wife, Joan Gardner-Taggart, who worried so much more about my thesis than her own that I was actually able to finish first. I think I'll have plenty of time to pay her back.

I. BACKGROUND

A. FEATURE TRACKING

From the first availability of sequential satellite images, researchers have been motivated towards estimating velocities of the atmosphere and ocean on a large scale from the motion of features in the images. The first attempts at estimating near-surface velocity fields in the ocean were by means of a technique called feature tracking.

Early feature tracking involved manually tracking the movement of patterns that could be easily identified in consecutive images. The displacement of the features between consecutive images was used to determine velocities. The identification and tracking of clouds in visible or infrared imagery has been used to calculate winds in the atmosphere. The movement of chlorophyll concentrations in Coastal Zone Color Scanner (CZCS) imagery and Sea Surface Temperature (SST) gradients in infrared imagery have both been used to estimate near-surface current velocities in the ocean.

Svejkosky (1988) found RMS error of 0.06 ms^{-1} between feature tracking derived velocities from Advanced Very High Resolution Radiometer (AVHRR) imagery and those obtained from sea surface drifters. The error was low because constraints on the feature tracking were restrictive, allowing use of only the most distinctive features and holding the temporal variation between the imagery and surface drifters to five hours.

There are several drawbacks to manual feature tracking. It is very time consuming and highly subjective. Different operators will achieve differing results from the same sets of imagery. Feature tracking cannot be used on low contrast or low gradient images since they have no features discernable to the human eye.

Feature tracking has been made more objective through computer automation. A technique developed by Leese et al. (1971) for cloud tracking was adapted for use with SST images by Emery et al. (1986). The Maximum Cross Correlation (MCC) technique involves cross correlating small sections in the first image with slightly larger sections in the second image. The cross correlated "windows" in each image have the same geographical center point. Displacement vectors from the window centers to their respective points of maximum correlation represent the surface velocity field.

The main drawback of the MCC technique is that it is adversely affected by the distortion and rotation of the features as they move. Additionally, the technique is unable to distinguish motion that is occurring parallel to the thermal or color gradients.

Tokmakian et al. (1990) achieved RMS errors of 0.18-0.23 ms^{-1} using the MCC technique with AVHRR images having 12 hour separations. They were able to better quantify the actual error in the MCC technique by applying the MCC technique to synthetic SST images. Synthetic SST images were produced by advecting the temperature field of an infrared satellite image with the velocity field of a numerical model and then sampling the model output at the desired intervals. The error of the MCC technique could then be found directly by comparing its velocities to the known velocities of the numerical model. Analysis indicated that the error might be reduced by cutting the image separation to 6 hours and by incorporating some means to account for rotation. They also felt that improvement might be realized by starting the correlative searches in high gradient regions and by somehow eliminating random, spurious high correlations that were occurring between distant, unrelated areas of the images.

B. INVERSE METHODS

A different objective approach to deriving near-surface velocities from AVHRR imagery is through the use of inverse methods. Wunsch (1978, 1985), Fiadeiro and Veronis (1982, 1984) and Roemmich (1979, 1981) are a few of those who have applied inverse methods to measured distributions of tracers in the ocean in order to infer large scale circulation and current velocities.

Generally speaking, inverse problems involve combining measurements of conserved properties and their corresponding governing equations into a mathematical system. The resulting system can be underdetermined or overdetermined and is solved using numerical methods for a velocity field which could have produced the measured distribution of properties.

A critical assumption in the subjective and objective feature tracking techniques described earlier was that the temperature gradients were being advected without significant change. This is actually not the case as surface heat fluxes, heat diffusion and vertical mixing of the water column all act to change the surface temperatures and gradients. Inverse methods would seem to be better suited to this problem because they better represent the actual physical processes involved. Source terms as well as other physics can be included in the model rather than assuming straight advection.

The relevant forward problem involving temperature advection and the heat equation is to calculate some future surface temperature field given an initial surface temperature field and a horizontally advecting velocity field. The corresponding inverse

problem is to determine the advecting velocity field given only the initial and final temperature fields. Even the forward problem in this case is not well understood since in reality it is a three-dimensional non-conservative problem. Kelly (1989) applied an inverse model to the heat equation and found good agreement between the model's velocity solutions and coincident Doppler Acoustic Log (DAL) data.[1] More detail concerning the inverse method with temperature advection and the heat equation will be presented in Chapter II.

C. RADAR ALTIMETER DERIVED NEAR-SURFACE VELOCITIES

An entirely different means of deriving near-surface velocities from satellite data is to use radar altimeter data. Radar altimeters accurately measure the distance from the satellite to the surface of the earth. Sharp pulses of electromagnetic radiation (at a frequency of 13.5 Ghz for the GEOSAT radar altimeter) are beamed towards the earth's surface and their travel time converted to distance. Corrections described in Cheney et al. (1987) for the GEOSAT altimeter are applied to the raw data to correct for tides, atmospheric water vapor, tropospheric and ionospheric delays and surface atmospheric pressure. Over the ocean, subtracting the satellite radar altimeter measurement from the height of the satellite's orbit results in the height of the sea surface relative to the center of the earth. Figure 1 illustrates these relationships. The sea surface height variability is due mainly to a combination of 1) the shape of the geoid, 2) ocean tides, and 3) ocean currents. Having already corrected for tidal effects, a correction must be applied for the variations due to the geoid in order to realize the sea surface height variations resulting solely from the ocean's currents.

The true geoid is the gravitational equipotential surface corresponding to the level the ocean would seek with gravity and centrifugal forces as the only forces acting upon it. Geoid variations range from -104 m to $+60$ m while the variations in dynamic height due to ocean currents are generally ± 1.5 m. Averaging the radar altimeter measurements of many orbits over the same location will determine an altimetric geoid. An altimetric geoid is often used as an approximation for the true geoid. Unfortunately, such time averaging includes sea surface height variations due to the mean flow of the ocean in the altimetric geoid. Other means can be used to find the true geoid over the ocean. The long wave components of the geoid can be found through their effect on

---

[1] The DAL is an earlier version of the Acoustic Doppler Current Profiler (ADCP) which will be described later. Both will be referred to as ADCP in this paper.

satellite orbits. The short wave components can be found through detailed gravity surveys. Once again difficulty arises because sufficiently detailed gravity surveys are available for only small areas of the world's oceans. Additionally, security classification restrictions have precluded the use of an accurate geoid in general scientific research (Stewart, 1985).

Roemmich and Wunsch (1982) describe ±10 cm as an attainable accuracy for a geoid obtained by using inverse methods with radar altimeter and hydrographic data to remove the mean oceanographic signal from an altimetric geoid. They also demonstrate that 10 cm is the maximum allowable error for a true geoid in order for it to be useful in improving estimates of the general circulation of the ocean.

Joyce et al. (1986) project a capability for significant improvement in the geoid through the use of inverse methods with a combination of hydrographic and ADCP velocity data. Near-surface geostrophic velocities obtained from the inversion would be used to calculate the dynamic height of the ocean's surface. The resulting dynamic heights would be used to further refine the geoid to accuracies not attainable using gravimetry.

The dynamic height variation of the ocean that remains after the final geoid correction is applied to the radar altimeter data. The dynamic height variation along the satellite track bears the following relationship to the cross-track geostrophic current velocity

$$\mathbf{u}_x = \frac{-g}{f}\frac{dh}{dy} \tag{1.1}$$

where $\mathbf{u}_x$ is the cross-track surface velocity, g is gravity, f is the Coriolis parameter and $\frac{dh}{dy}$ is the dynamic height variation along the satellite track. The accuracy of radar altimeter derived geostrophic velocities is related to the accuracy of the geoid through its effect upon the accuracy of the dynamic height field.

Kelly and Gille (1990) used information from the GEOSAT radar altimeter to calculate Gulf Stream velocities that were in good agreement with shipboard ADCP measurements. They subtracted the mean of all of the height profiles as a substitute for a reference geoid in order to get GEOSAT residual height profiles. A theoretical model of the Gulf Stream velocity profile was used to generate synthetic height profiles. The synthetic height profiles were then added to the GEOSAT residual height profiles in order to account for the mean flow of the Gulf Stream. They achieved an RMS error of

0.23 ms^{-1} between a GEOSAT derived velocity profile and one that had been measured with an ADCP four days earlier. Most of the error was attributed to the temporal variability of the Gulf Stream evidenced through sequential ADCP profiles.

D. RADAR ALTIMETER DERIVED VELOCITIES AS CONSTRANTS ON AN INVERSE MODEL

The system of equations and unknowns comprising an inverse model may be supplemented by known data. Such a system is said to be constrained by the known data which acts to guide the inverse model towards a solution that is representative of the known data. This project will evaluate the effects of adding simulated radar altimeter derived velocity data as an additional constraint to the inversion.

II. METHODS

Kelly (1989) applied an inverse model using AVHRR imagery as input to the heat equation

$$T_t + \mathbf{u} \cdot \nabla T = \kappa \nabla^2 T + S \tag{2.1}$$

where T is temperature, u is velocity, κ is a diffusion coefficient, S is a source term and subscripts denote partial differentiation.

The horizontal temperature gradients were computed from 256x256 pixel images by a linear least-squares fit across 16x16 pixel tiles. With an AVHRR sensor footprint of 1.15 km the resulting $\simeq$ 18x18 km boxes could sustain a maximum cross-isotherm velocity of 15 kmd^{-1} over a one day time separation without violating the Courant-Friedrich-Lewey (CFL) criterion $\Delta x > u\Delta t$. The term T_t was approximated by the finite difference $\frac{\delta T(x,y)}{\delta t}$ for sequential images separated in time. A small correction for bias in the images was made by calculating a mean image temperature difference using only low gradient tiles. That mean was then subtracted from the temperature difference calculated for each tile. In other words, the low gradient regions were assumed to be constant temperature and any temperature change occurring in those regions over the image interval was assumed to be bias in the images. The source term S accounted for surface heat fluxes and vertical entrainment which were assumed to vary slowly over the image. It also included large scale temperature error introduced into the satellite imagery by atmospheric effects. Diffusion was neglected as being at least an order of magnitude smaller than advection.

Considering $\mathbf{u}$ as across and along isotherm components showed that the advective temperature change was due to the cross isotherm component only.

$$\mathbf{u} \cdot \nabla T = (\mathbf{u}_c + \mathbf{u}_a) \cdot \nabla T = \mathbf{u}_c \cdot \nabla T \tag{2.2}$$

Since there was no contribution to advection by $\mathbf{u}_a$ (or either component where there were negligible temperature gradients) an infinite number of solutions to 2.1 existed. In order to achieve solutions that were unique but also physically reasonable, limitations on the divergence, energy and vorticity of the inversion solution were chosen as

constraints on the problem. The equation to be minimized was (Kelly, 1989)

$$\sum_{i,j}\left[\,|\,T_t+\mathbf{u}\cdot\nabla T-S\,|_{i,j}^2+\alpha^2\,|\,\nabla\cdot\mathbf{u}\,|_{i,j}^2+\beta^2\,|\,\mathbf{u}\,|_{i,j}^2+\gamma^2\,|\,\nabla\times\mathbf{u}\,|_{i,j}^2\right] \tag{2.3}$$

where $T_t+\mathbf{u}\cdot\nabla T-S$ is the heat equation with diffusion neglected, $\nabla\cdot\mathbf{u}$ is the divergence, $\mathbf{u}^2$ is the energy and $\nabla\times\mathbf{u}$ is the vorticity of the solution. Weighting factors α, β and γ are used to specify the relative importance of each constraint to the inversion.

Minimization of divergence forced temperature changes to be made through movement of features rather than by convergence/divergence. Minimizing the energy of the solution most closely approached the solution allowing only cross-isotherm flow. A minimum vorticity solution allowed jets only where necessary to satisfy the heat equation.

The resulting overdetermined system of the heat equation and constraints was solved using a matrix factorization algorithm. The algorithm used least squares methodology in order to satisfy all equations as equally as possible.

Testing of the inverse model was done using synthetic images with synthetic velocity fields and then real images with synthetic velocity fields. The purpose of the tests was to find the proper weightings for the divergence and energy constraints as well as determine the model's sensitivity to some types of expected error.

For the first test, a relatively low gradient ($< 0.1°\text{Kkm}^{-1}$) synthetic temperature image was advected by a variety of uniform or slightly divergent synthetic velocity fields ($V_{max} \simeq 15$ kmd^{-1}). The temperature differences of the resulting images were then input to the model. Varying the weights on the constraints revealed their effects on the inverse model in terms of percent misfit of the model's solution to the actual time-rate of temperature change. Analysis indicated that the main source of error when utilizing "perfect" data was underparameterization of the velocity field by the four term Fourier expansion. Solution velocities were also lower than the actual velocities due to the low gradients of the synthetic temperature image. Negligible temperature changes between the images did not require advecting velocities in order to solve the heat equation.

The second test involved the advection of a real temperature image with a divergent synthetic velocity field. The best solutions from that test had lower divergence and energy than the actual solution. There was also a tendency for the model to develop spurious structure in the solutions. The velocity error was smaller however for the solutions in the second test sequence because the real image had stronger gradients than

the synthetic image used in the first set of tests. Noise calculated on the basis of imagery calibration error analysis was then added to the test data. Solutions again had lower divergence and energy than the actual solution.

For inversions with real data, weights on the constraints were chosen to yield a family of solutions within a certain range of temperature misfit values. The acceptable range of misfit values was determined from estimates of the image calibration error and the small-scale temperature error estimated from the model's large-scale source terms S. Inversions performed on real images produced solutions that were for the most part qualitatively correct with respect to coincident ADCP data but having lower velocities, divergence and energy.

Additional weighted constraints in the form of known velocities or estimated velocities from another data source could also be added to the system. If the known or estimated velocities happened to be representative of the actual along isotherm velocities, significant improvement should be realized over the inversion alone.

III. DATA

A. AVHRR IMAGERY

The AVHRR images used for this project were four clear, consecutive images from the NOAA 11 satellite. They were collected 12 hours apart over the period 16-17 July 1988 (Julian dates 198 and 199). Images from the NOAA 10 satellite were also available for this period but were not used because the NOAA 10 AVHRR lacked the Channel 5 data necessary to use the Multi-channel Sea Surface Temperature (MCSST) algorithms. Table 1 provides information pertinent to the imagery. The images can be seen as the backgrounds for the Coastal Transition Zone (CTZ) ADCP velocity field (Figure 6) and the inversion-alone solutions (Figures 7-9).

Table 1. NOAA 11 AVHRR IMAGERY

Image Designation	Julian Date	Time of Pass		Satellite Zenith Angle	CTZ Temperature Statistics		
		GMT	Local		T_{max} (°C)	T_{min} (°C)	T_{avg} (°C)
19812	198	1200	0500	35°	17.8	7.1	14.6
19823	198	2300	1600	3°	17.4	7.5	13.9
19912	199	1200	0500	45°	18.9	7.0	13.9
19923	199	2300	1600	18°	18.4	7.9	13.7

The images were navigated by Mark Abbott at Oregon State University to an accuracy of ± 1 pixel using Global Imaging, Inc. satellite data processing software. The current National Environmental Satellite, Data and Information Services (NESDIS) operational MCSST algorithms for the NOAA 11 satellite were used to calculate sea surface temperatures from the AVHRR Channel 4 and 5 radiances. Values outside the range 7-19°C were masked and rejected as not being representative sea surface temperatures. That range was based on data from Huyer et al. (1990) for the Coastal Transition Zone (CTZ) during this time, expanded to account for the AVHRR RMS temperature error of 0.5°C reported by McClain et al. (1985).

No cloud masking was done on the images because of their high clarity. There was an area of clouds in Image 19812 that covered a small area of the extreme southwest

corner of the model grid. The clouds did result in erroneous velocities from the inverse model in that region. There also appeared to be coastal fog present in Images 19823, 19912 and 19923. The presence of fog would account for the abnormally high nearshore velocities in some of the model solutions using those images.

B. CTZ DATA

The control data for this project consisted of Acoustic Doppler Current Profiler (ADCP) and Conductivity, Temperature and Depth (CTD) data collected for the Coastal Transition Zone (CTZ) Field program over the period 13-18 July 1988 by the R/V PT SUR. Table 2 summarizes the temporal aspects of the CTZ88 Grid II ADCP data, collected in seven northwest-southeast transects labelled A-G.

Table 2. CTZ88 GRID II ADCP SURVEY

Line	Date (1988)	Time (GMT)	
		Start	End
A	13-14 July	0813	0201
B	14 July	0446	1945
C	14-15 July	2211	1015
D	15-16 July	1239	0215
E	16-17 July	0504	0124
F	17 July	0417	2000
G	17-18 July	2346	1515

The ADCP velocity field and dynamic height fields of the CTZ during this period (Figures 2 and 3) show good agreement. The dominant feature in both data sets is a strong surface jet extending northeast to southwest across the study region, with maximum speeds reaching $\simeq$ 90 cms^{-1}. The circulation in the northwest corner is weakly cyclonic. A weaker onshore "return" flow exists to the south of the main jet.

An ADCP measures current velocity at various depths (bins) by range-gating a sonar pulse and recording the Doppler shift of the signal returned from each bin (Figure 4). Calculation and subtraction of the effects of the ship's motion from the total Doppler shift velocity leaves the velocity due to the motion of scatterers in the ocean. The scatterers are presumed to be drifting with the current. Averaging over some optimal length of time yields a mean current for each depth bin over an area corresponding to the distance travelled by the ship over the averaging time. Error in the ADCP velocity

is mainly due to signal processing difficulties arising from the orders of magnitude difference that can exist between the actual currents and the ship's speed. Other error results from the ship's motions due to wave action and the detrimental effects of navigation error on calculations of the ship's speed (Kosro, 1985).

C. SYNTHETIC GEOSAT-DERIVED VELOCITY DATA

Synthetic GEOSAT-derived velocity data, generated from ADCP control data, was used as an additional constraint on the inversion. The cross-track ADCP data were averaged over a time interval that approximated the 7.5 km sensor footprint of GEOSAT. The ADCP survey lines were used to simulate GEOSAT ground tracks. The line spacing of the ADCP survey was 25 km compared to the $\simeq$ 130 km track spacing of repeat GEOSAT orbits over the CTZ. The angle between the ADCP survey lines and the model grid was 30° while the angle between the GEOSAT ground tracks and the model grid would have been $\simeq$ 25°. Figure 5 shows the synthetic GEOSAT-derived velocity field.

The error of the ADCP data set was estimated at 5-10 cms^{-1} by Huyer et al. (1990). Since the synthetic velocity data was derived from actual velocity data rather than synthetic raw altimeter data or synthetic dynamic height profiles, any error normally incurred in the process of converting raw altimeter data to geostrophic velocities was avoided. The availability of an accurate geoid was not a factor and no estimate of the geoid was made. Although the ADCP data was collected over time and therefore was not coincident to all of the image pairs used with the model, for the purposes of this study, the synthetic velocity data were assumed to be coincident with the imagery.

IV. THE MODEL

The model used was essentially the same one used and described in Kelly (1989). The model had been previously modified to accept known velocities in the form of ADCP data which was weighted and used as a constraint on the inversion. The newer model lacked the vorticity constraint of the earlier model which was removed because it had only a minor effect on the results. Additionally, the newer model parameterized the velocities as biharmonic splines rather than as Fourier coefficients. The use of biharmonic splines reduced the tendency of the solution to resonate around areas where data were masked (Kelly, personal communication).

In order to incorporate the synthetic GEOSAT-derived velocity data as a constraint on the inversion, the model was further modified to minimize the difference between the velocity component normal to the satellite track and the inversion velocity. The inversion velocities were free to vary in the direction of the unknown component along the satellite track. The family of equations described in 2.1 became

$$\sum_{i,j}\left[\,|\,T_t+\mathbf{u}\cdot\nabla T-S\,|_{ij}^2+\alpha^2\,|\,\nabla\cdot\mathbf{u}\,|_{ij}^2+\beta^2\,|\,\mathbf{u}\,|_{ij}^2+\eta^2\,|\,v_s-(u\cos\theta+v\sin\theta)\,|_{ij}^2\right] \qquad (4.1)$$

where the terms are as described in 2.1 with the addition of another weighting function (η), the synthetic GEOSAT cross-track velocity component (v_s) and the angle between the model's grid and the satellite track (θ).

V. RESULTS

A. THE INVERSE MODEL WITHOUT VELOCITY CONSTRAINTS

The modified model was run without velocity constraints. The resulting velocity fields were products of the inversion alone with constraints only on the divergence and energy of the solution. The model was run on each of the three image pairs with 12 hour separations and also on the two image pairs with 24 hour time differences.

The weights on the divergence and energy of the solution (α^2 and β^2 in equation 2.3) were held constant at .01 and .03 for all model runs. These values were used because they gave qualitatively good results and project time constraints precluded a search for weights that might have yielded better solutions. Better results (quantitative reductions in the velocity error between the model output and known solutions) may be possible through further optimization of α and β.

Several characteristics were calculated for each of the velocity solutions in order to allow quantitative comparisons. The energy and divergence of each velocity solution were computed. A percentage temperature error for each velocity solution was computed using the following equation:

$$T_{err} = \sum_{i,j} \left[\frac{| T_t - ((\mathbf{u} \cdot \nabla T) + S) |_{i,j}^2}{| T_t |_{i,j}^2} \right] \tag{5.1}$$

where T_t is the temperature difference between the image pairs, $\mathbf{u}$ is the model's velocity solution, ∇T is the computed image gradient, S is the source terms calculated by the model and $i=j=16$. A percentage velocity error between the model velocity solution and the CTZ88 Grid II ADCP velocity field was calculated in the following manner

$$V_{err} = \sum_{n} \left[\frac{(u_a - u_m)^2 + (v_a - v_m)^2}{(u_m + v_m)^2} \right] \tag{5.2}$$

where n (= 75) was the number of tiles where measured velocity data existed and subscripts a and m denote ADCP and model velocities respectively. Table 3 provides a

summary of the characteristics of the solutions using the inversion without any known velocities as constraints. Figure 6 is the CTZ88 Grid II ADCP velocity field overlaid on Image 19823. Figures 7-11 are the velocity fields from the inversion alone overlaid on either the second image of the pair used, or the image at the midpoint of the interval between the image pair.

Table 3. CHARACTERISTICS OF INVERSION-ALONE SOLUTIONS

Image pair	Energy (km^2d^2)	Divergence (d^{-1})	T_{err} (%)	V_{err} (%)
19812-19823	180.0	0.316	5.94	92.4
19823-19912	259.0	0.421	34.20	107.0
19912-19923	293.0	0.579	7.76	101.0
19812-19912	107.0	0.314	11.20	97.9
19823-19923	96.6	0.276	7.39	96.0

The strong jet from the CTZ88 Grid II ADCP and dynamic height fields (Figures 1 and 2) is also evident in the AVHRR imagery. The cyclonic eddy is also apparent to the west of the cold front near Point Arena. The eddy is partially included in the northeast quadrant of the model grid although it is not well sampled by the CTZ88 Grid II ADCP survey. In all cases, the inverse model when used alone appeared to have problems handling the jet. The solutions do show some of the convergence necessary for the formation of the jet, but don't actually define it. Part of the difficulty may have been due to the narrowness of the cold filament in relation to the scale of the model grid and because the jet velocities were predominately along-isotherm.

Looping the images revealed movement that was not readily discernable from the still pictures. Over the sequence of images, the middle north-south oriented portion of the cold front translated westward $\simeq$ 18 km, a distance roughly equal to its width. The east-west oriented region of the cold filament remained nearly stationary and appeared to narrow and get colder over the image sequence. The looped sequence also showed the growth and southeastward movement of the northern cylconic eddy. The movement of the filament over the interval between images appeared to have weakened the average gradients computed by the model causing it to inadequately define the jet in that area, producing the velocity "holes" in the center of most solutions. In other words, the

inversion-alone vectors in many cases were simply an accurate representation of the cross isotherm velocities (translation of features).

The inversion-alone solution for image pair 19812-19823 (Figure 7) gave the best quantitative results in terms of lowest temperature and velocity error (Table 3). It also looked the best qualitatively because of its lack of erroneous structure in the low gradient regions. The solution did have the "hole" associated with the narrow east-west section of the jet. Erroneous velocities were present in the extreme southwestern corner of the model grid owing to the cloud contamination in Image 19812. The possible presence of coastal fog could also call into question some of the nearshore velocities.

The solution for image pair 19823-19912 (Figure 8) had the largest temperature and velocity errors of the inversion-alone solutions. This image pair had the largest change in T_{max} between any of the pairs as well as the second largest change in T_{min} (Table 1). This temperature change is the opposite of what would be expected from any diurnal effect resulting from the 12 hour day/night image separation. This image pair also has the largest satellite zenith angle difference (Table 1) of any of the pairs. The zenith angle difference or alternatively just the large satellite zenith angle of Image 19912 could be causing a problem through the MCSST algorithm used in these cases. The $\simeq$ 9 km westward translation of the north-south section of the jet between the images was the largest of any of the pairs. The area of the bend from north-south flow to east-west flow also translated southeastward. These feature translations could be responsible for the strong eastward (cross-jet) velocities over the north-south segment of the jet and the seemingly erroneous southward velocities in the low gradient region to the north and west of the bend in the jet. The noise present at the bottom of Image 19912 was rejected as out-of-range temperatures and did not have any effect on the model.

Image pair 19912-19923 produced a solution (Figure 9) that fell between the preceding two descriptions. Feature translation did not appear to occur between the images in this instance but there were rather severe problems with erroneous velocities in the relatively low gradient region to the west of the jet.

Feature translation appeared to be the largest error source in the solutions using 24 hour separation (Figures 10 and 11). In these cases the greater image temporal separation allowed the features to translate further over the interval between images. As expected considering the previous results, the solution involving Image 19912 (Figure 11) had the worst characteristics. Although no diurnal effects were apparent in any of these cases, the 24 hour image separation would minimize any adverse effects that a diurnal temperature variation would have on the inverse model.

B. THE INVERSE MODEL WITH SYNTHETIC VELOCITY CONSTRAINTS

The next step was to add the synthetic GEOSAT-derived velocity data as an additional constraint on the inversion. The modified model was run and various combinations of the synthetic velocity data lines B-G were added to the problem. The actual energy of the CTZ88 Grid II ADCP velocity field was calculated to be $\simeq$ 875 km^2d^{-2}, however velocity solutions from the model with this energy level tended to spread the energy from the jet over the entire model grid and added erroneous structure in areas where the temperature gradients did not support it. The data weights (η) were incrementally varied for each individual case. A weight was then chosen for each case to optimize a solution in the energy range 200-300 km^2d^{-2}, in order to achieve solutions that were the most qualitatively correct with respect to the imagery and the CTZ88 Grid II ADCP velocity data. The values for η varied from .03-.49 with the weights in 15 of the 23 cases falling in the range .03-.06.

Tables 4-8 show the characteristics of the solutions resulting from the addition of various combinations of the lines of synthetic velocity data as additional constraints on the inversion.

Table 4. CHARACTERISTICS OF 19812-19823 WITH VELOCITY CONSTRAINTS

Data Lines Added	Energy (km^2d^2)	Divergence (d^{-1})	T_{err} (%)	V_{err} (%)
none	180.0	0.316	5.94	92.4
E	255.0	0.389	6.10	92.1
DE	253.0	0.376	6.05	88.6
DEF	271.0	0.362	6.05	87.9
EFG	253.0	0.345	6.00	89.0
D-G	271.0	0.330	6.01	86.2

There was no significant change in the percent temperature error, which in some cases actually got slightly larger by 1-2%. This was not entirely unexpected since the velocity constraints could act to produce a solution different from the most thermodynamically correct one. The velocity error was large for all solutions (80-100%) but was improved by 10-15% in some cases by the addition of the known velocity constraints (image pairs 19812-19823, 19912-19923, 19812- 19912 and 19823-19923).

Table 5. CHARACTERISTICS OF 19823-19912 WITH VELOCITY CONSTRAINTS

Data Lines Added	Energy (km^2d^2)	Divergence (d^{-1})	T_{err} (%)	V_{err} (%)
none	259.0	0.421	34.20	107.0
F	311.0	0.494	34.80	110.0
EF	318.0	0.433	34.20	106.0

Table 6. CHARACTERISTICS OF 19912-19923 WITH VELOCITY CONSTRAINTS

Data Lines Added	Energy (km^2d^2)	Divergence (d^{-1})	T_{err} (%)	V_{err} (%)
none	293.0	0.579	7.76	101.0
F	383.0	0.654	7.91	103.0
FG	380.0	0.612	7.82	102.0

Table 7. CHARACTERISTICS OF 19812-19912 WITH VELOCITY CONSTRAINTS

Data Lines Added	Energy (km^2d^2)	Divergence (d^{-1})	T_{err} (%)	V_{err} (%)
none	107.0	0.314	11.2	97.9
E	244.0	0.454	13.8	102.0
EF	244.0	0.420	13.1	104.0
DEF	236.0	0.407	12.7	98.3
EFG	243.0	0.380	12.4	96.9
C-F	234.0	0.417	12.6	96.9
D-G	256.0	0.368	12.4	94.3
B-G	229.0	0.347	12.6	90.4

Table 8. CHARACTERISTICS OF 19823-19923 WITH VELOCITY CONSTRAINTS

Data Lines Added	Energy (km^2d^2)	Divergence (d^{-1})	T_{err} (%)	V_{err} (%)
none	96.6	0.276	7.39	96.0
E	232.0	0.430	8.87	98.3
EF	224.0	0.413	8.36	98.7
DEF	226.0	0.389	8.42	90.3
EFG	228.0	0.354	8.03	90.5
C-F	231.0	0.416	8.47	89.9
D-G	247.0	0.332	8.35	86.2
B-G	232.0	0.330	8.83	83.5

Adding the velocity data greatly improved the ability of the model to reproduce mesoscale features that were apparent in the in situ data. This was demonstrated by the data addition sequence for image pair 19812-19823 in which velocity data was cumulatively added to the inverse model (Figures 12-16). Data line E was generated from the ADCP data most coincident to this image pair with data lines D and F the next most coincident. The addition of just one line of synthetic velocity data significantly improved the definition of the jet by eliminating the "hole" in the middle of the inversion-alone solution (Figure 12). Steady improvement resulted from the addition of more data (Figures 13-16) but the biggest qualitative improvement came through the addition of just line E. Figures 12 and 16 look almost the same. The model jet was wider (55 vs 74 km) than the jet observed in the ADCP data (Figure 2) and located a bit further to the north. The model also failed to produce any indication of the return flow to the south of the jet and had some erroneous nearshore velocities to the south of Point Arena. The missing return flow was likely due to a lack of strong gradients in the warmer water of the return flow region, and the nearshore problems could be attributable to coastal fog. The best percent misfit to the actual velocity data (83%) was achieved by using all of the synthetic velocity data with image pair 19823-19923 (Figure 17). Comparing this with the best results from image pair 19812-19923 (Figure 16) showed the two solutions to be qualitatively similar, but differing in detail. Figure 16 produced a better representation of the anticyclonic eddy in the northwest,

while Figure 17 had a more coherent convergent flow leading into the jet from the north. Although Figure 17 could appear to have too much energy, the fact that velocity comparisons were done only at points where ADCP data existed would allow that solution to be quantitatively the best but perhaps be qualitatively lacking. The solution from this image pair resulting from the addition of data lines D, E and F was considered to be the most qualitatively correct (Figure 18). The jet in the vicinity of the cold filament was well defined but more narrow than in some of the other solutions. Additionally, spurious structure in the low gradient areas of the images was kept to a minimum.

Relatively poor results are depicted in Figures 19 and 20. The inversion-alone solution in this case was the worst of the five cases, having the largest temperature and velocity errors. Possible reasons for the large errors were discussed in the previous section. Predictably, addition of the synthetic velocity data to the problem did little to improve it.

A drawback to this technique was that it only constrained the velocity component normal to the synthetic GEOSAT track. Descending GEOSAT orbits cannot be used near the western coast of the United States owing to data problems as the satellite transitioned from over land to over water. For this and other similar coastal areas, descending orbit data that would help define the radar altimeter derived current velocities would not be available and only one velocity component could be determined. Fortuitously, this synthetic data was nearly normal to the isotherms and the jet axis thereby providing the most needed (along-isotherm) information.

Another slighly unrealistic aspect of the synthetic data was its physical and temporal density. The spacing of the tracks in this project was 25 km as compared to the $\simeq$ 130 km spacing of GEOSAT ground tracks. There would also have been some temporal spacing to the GEOSAT ground tracks. This means that only one line of actual data would be really useful in combination with the inverse model and its utility would be directly related to the temporal separation between the GEOSAT data and the imagery used with the inverse model. Use of more than one track of GEOSAT data would requre additional temporal weighting on the second and subsequent tracks that would likely cause them to have negligible effect on the inverse model.

VI. CONCLUSIONS AND RECOMMENDATIONS

An inverse model using the heat equation with AVHRR imagery and constraints on the divergence and energy of the solution and with additional constraints in the form of synthetic GEOSAT-derived geostrophic current velocities showed promise as a means of improving the determination of near-surface current velocities entirely by remote means. In most of the cases run, both qualitative (visual comparison of current vectors) and quantitative (percent misfit to known velocities) improvement in the model's velocity solutions was obtained when synthetic velocity data was added. The model performed best with an image separation of 12 hours which minimized the translation of features over the interval between images. Excessive feature translation between the images smeared the temperature gradients resulting in incorrect velocities in the model's solutions. The physical effects of the addition of the synthetic velocity data did not spread much beyond the actual points at which it was added. For this reason, the qualitative improvement in some cases appeared to be better than was indicated by the quantitative measurements. There was also a tendency for the synthetic velocity data to misrepresent the jet since the ADCP data was collected over a six day period during which the jet location was changing.

The narrowness and orientation of the jet with respect to the model grid appeared to cause "holes" in the model's solutions. The model's apparent problem in these cases with the small width of the cold filament could be resolved by changing the model's tile size. With an image interval of 12 hours, 8x8 pixel tiles could be used without violating the CFL criteria discussed in Chapter I. Halving the tile size would double the size of the coefficient matrix with a concommitent increase in the computer processing time for the model.

The model could be improved for this data set by experimenting with the weights on the divergence and energy constraints (α and β) in order to find a set that improved the inversion-alone solutions. This is a process that would lend itself well to automation. Iterative computer techniques could be used to select weights for the constraints based on misfit levels chosen as a result of error analysis performed on the temperature data and the radar altimeter derived velocity data. It remains to be seen whether divergence and energy weights must be chosen for each image pair or whether one set of weights can apply to a set of images closely spaced in time or even closely related through similar

gradients. Using the inverse model with synthetic data generated by advecting a real image with a more sophisticated numerical model than that used by Kelly (1989) may help refine the selection criteria for the weights on the inversion constraints.

Another possible improvement would be to weight the velocity data constraints based on the sine of the angle between the satellite track and the temperature gradients. This would allow only the model to define the cross-isotherm velocities when the radar altimeter track was parallel to the temperature gradients. Conversely, when the track was normal to the temperature gradients, only the radar altimeter derived velocities would drive the along-isotherm velocities which are in the model's null space.

In order to incorporate real radar altimeter-derived geostrophic velocities into the model, a temporal weighting scheme would have to be used on the velocity data, such that radar altimeter data most coincident in time with the AVHRR data are weighted more than the less synoptic data.

The value of an operational system based on these methods increases in direct proportion to the amount and accuracy of data available. Future refinements to the geoid will increase the accuracy of the geostrophic velocities obtainable from radar altimeter data. Follow-on radar altimeters to GEOSAT may have better temporal and physical track separation which would result in more altimeter data coincident to any set of sequential infrared imagery. More than one altimeter in orbit would increase the accuracy of such a system even more by providing multiple coincident altimeter tracks per AVHRR image. Closely coincident tracks from ascending and descending orbits would be nearly normal to one another, allowing computation of velocity vectors rather than just the one normal component used in this project.

APPENDIX A. FIGURES

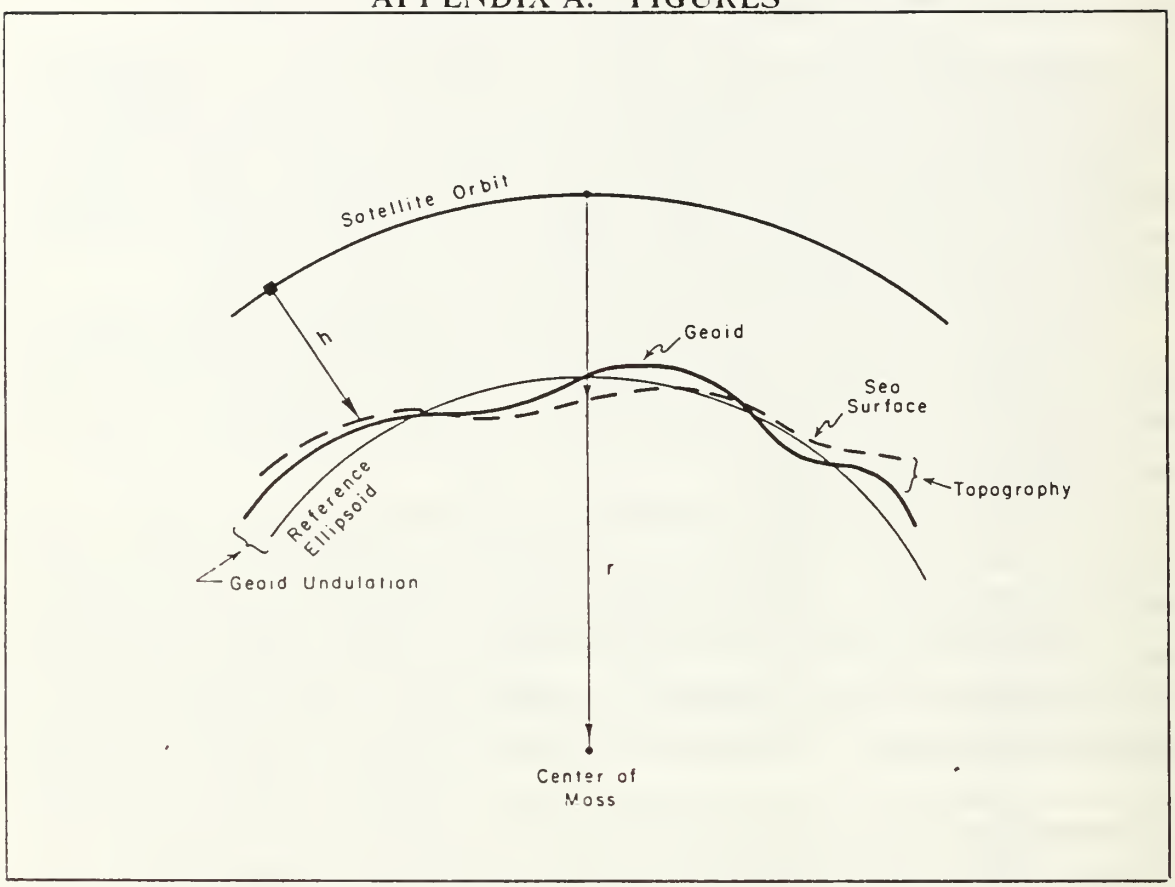

Fig. 1. Satellite altimetry relationships: Satellite height h subtracted from the satellite orbit height r yields the variation of sea surface height relative to the center of the earth. The reference ellipsoid is the best smooth approximation to the geoid. [After Stewart, (1985)]

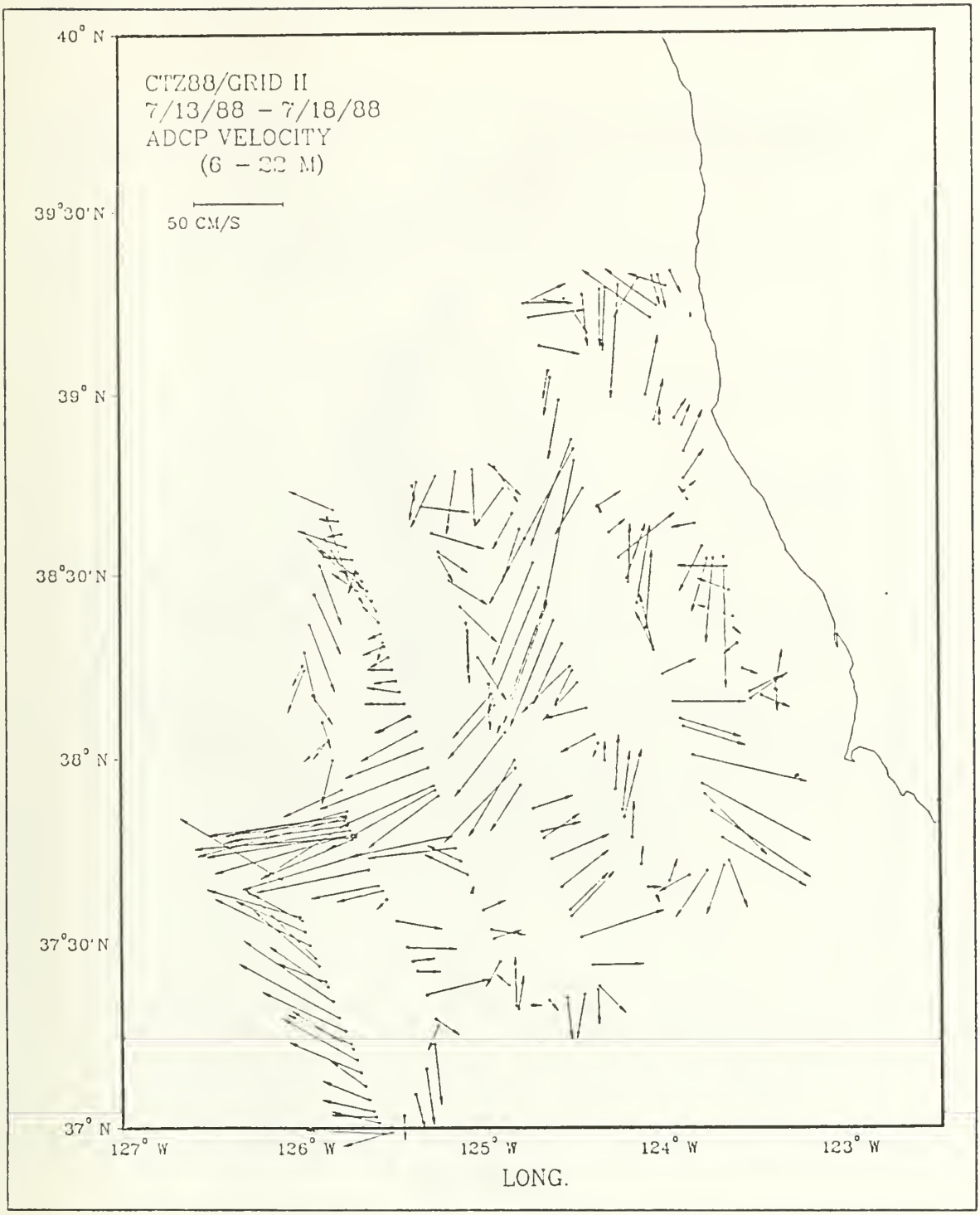

Fig. 2. ADCP velocity field from CTZ88 Grid II: [After Huyer et al., (1990)]

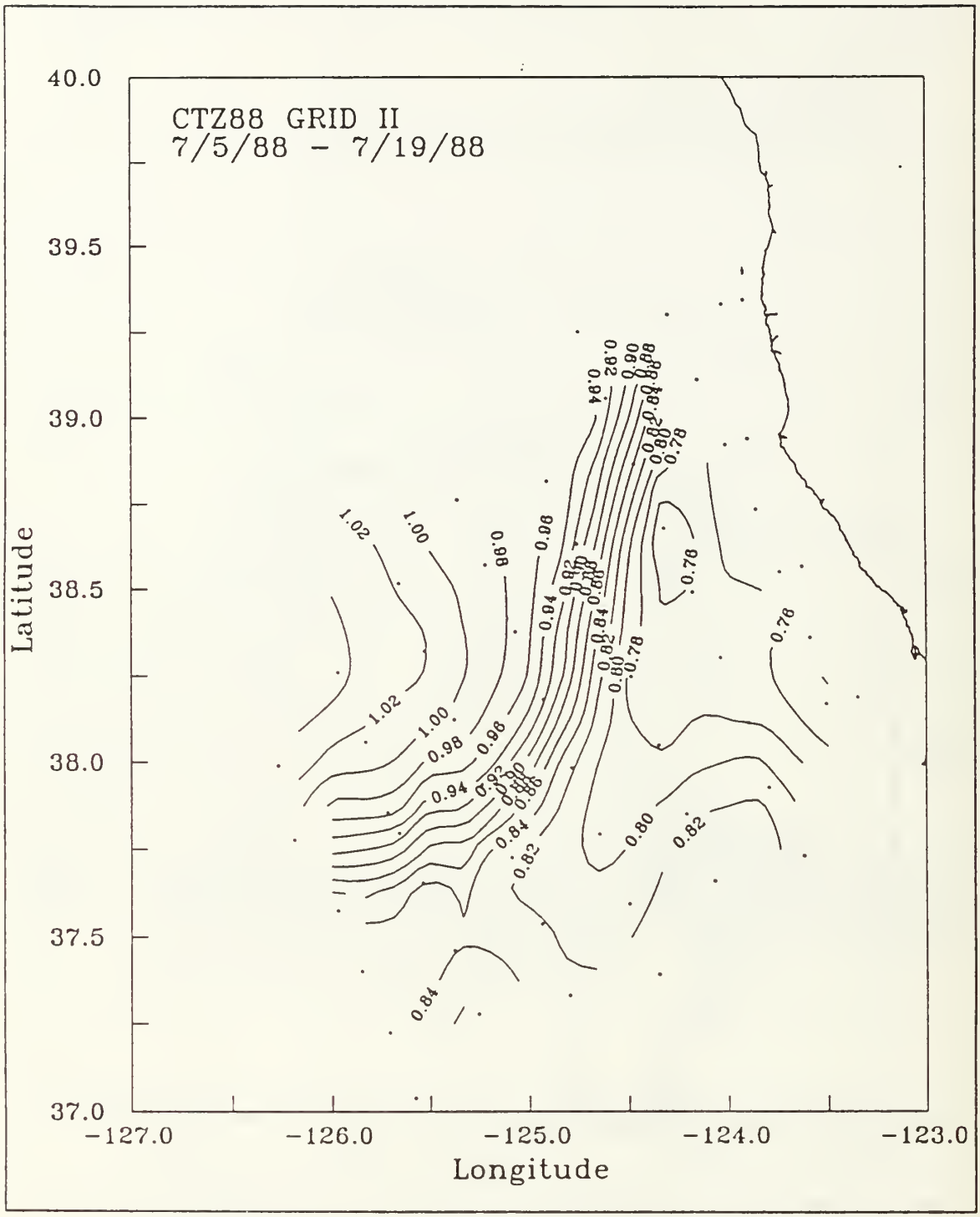

Fig. 3. Dynamic height field from CTZ88 Grid II: [After Huyer et al., (1990)]

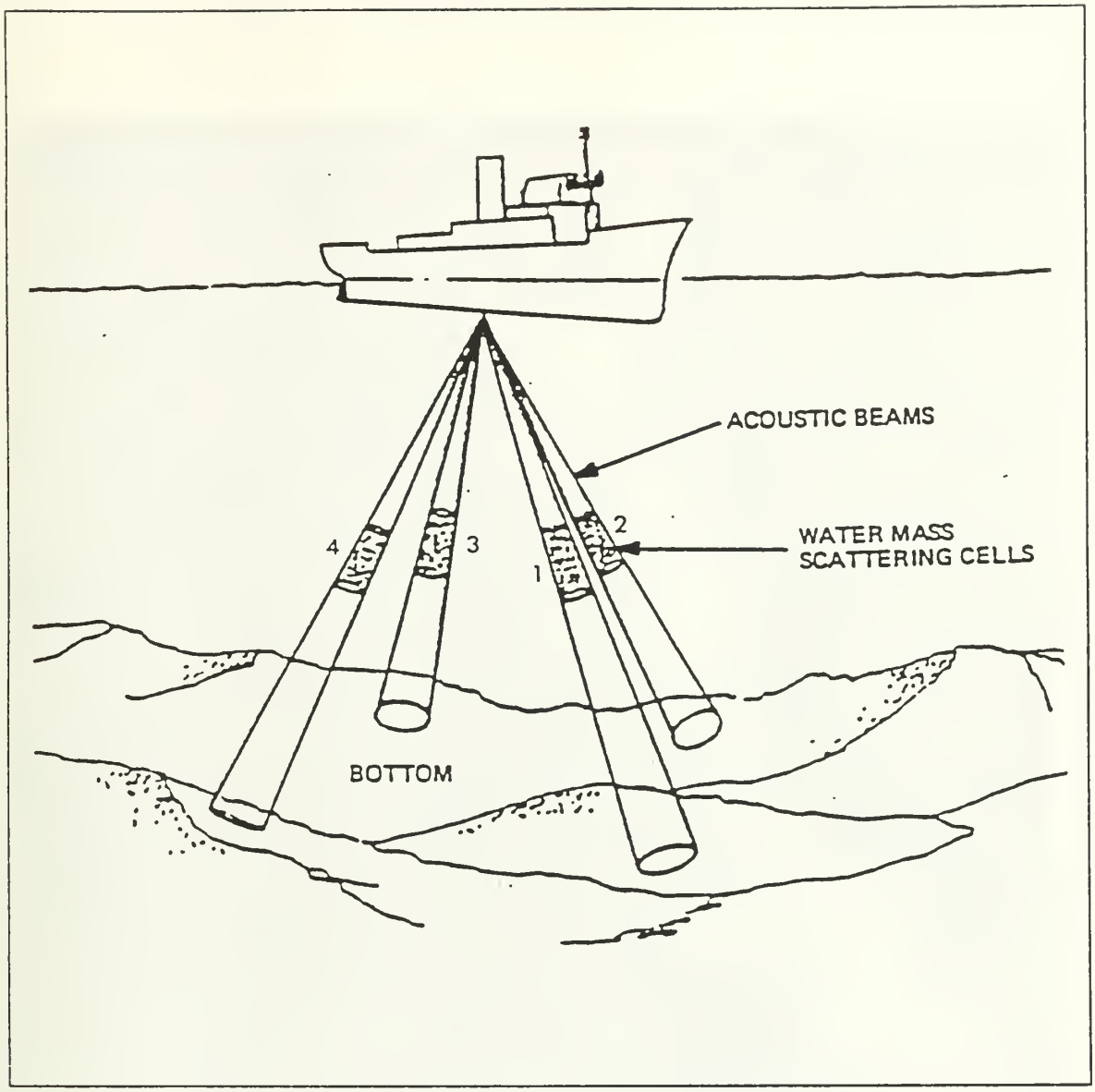

Fig. 4. Acoustic Doppler Current Profiler (ADCP) operation: The Doppler shift of the backscattered signal of the four beams measures the relative velocity between the ship and the ocean. Range-gating the signal allows determination of currents at different depths. [After Kosro, (1985)]

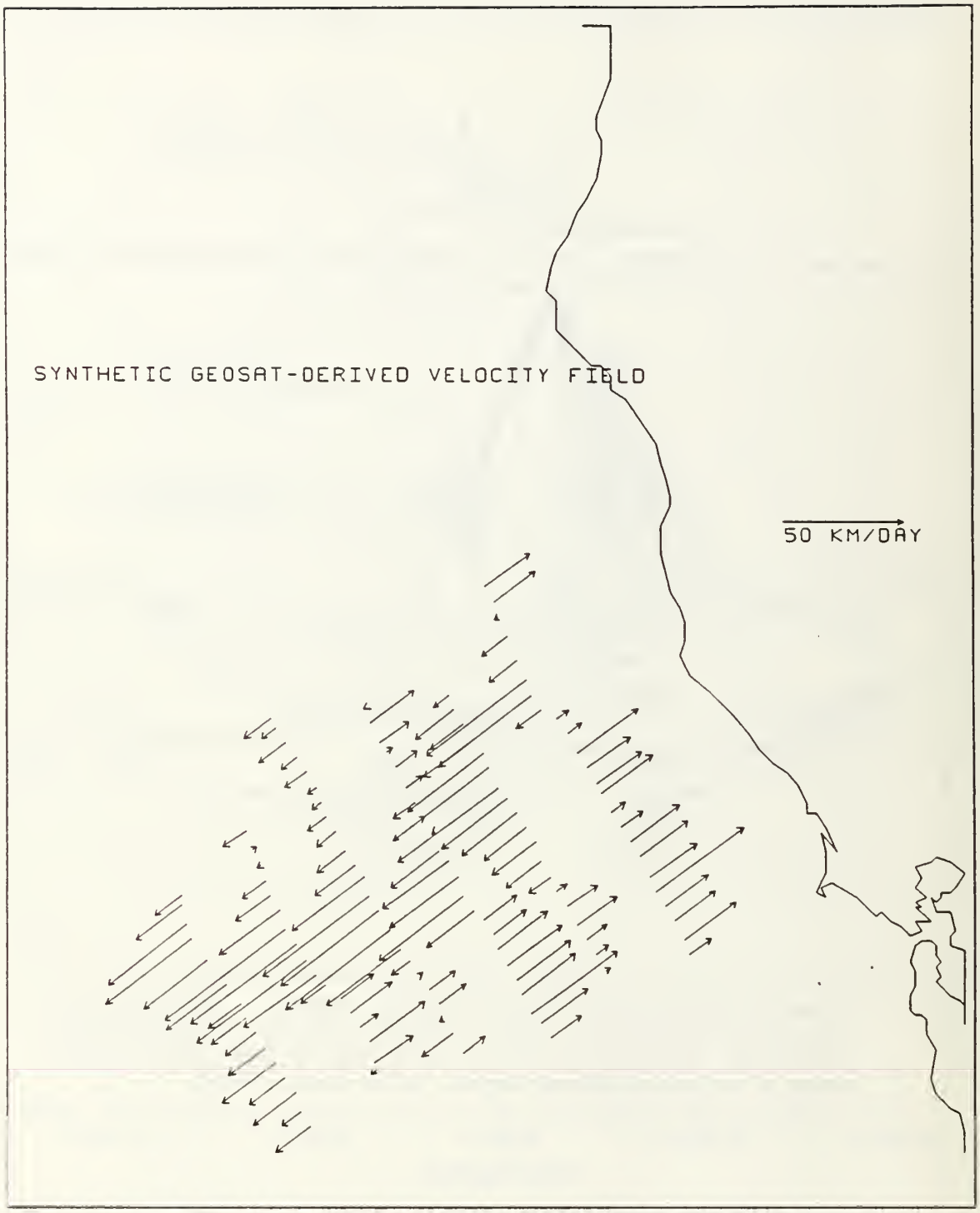

Fig. 5. Synthetic GEOSAT-derived velocity field: Line B is to the northwest proceeding to G in the southwest

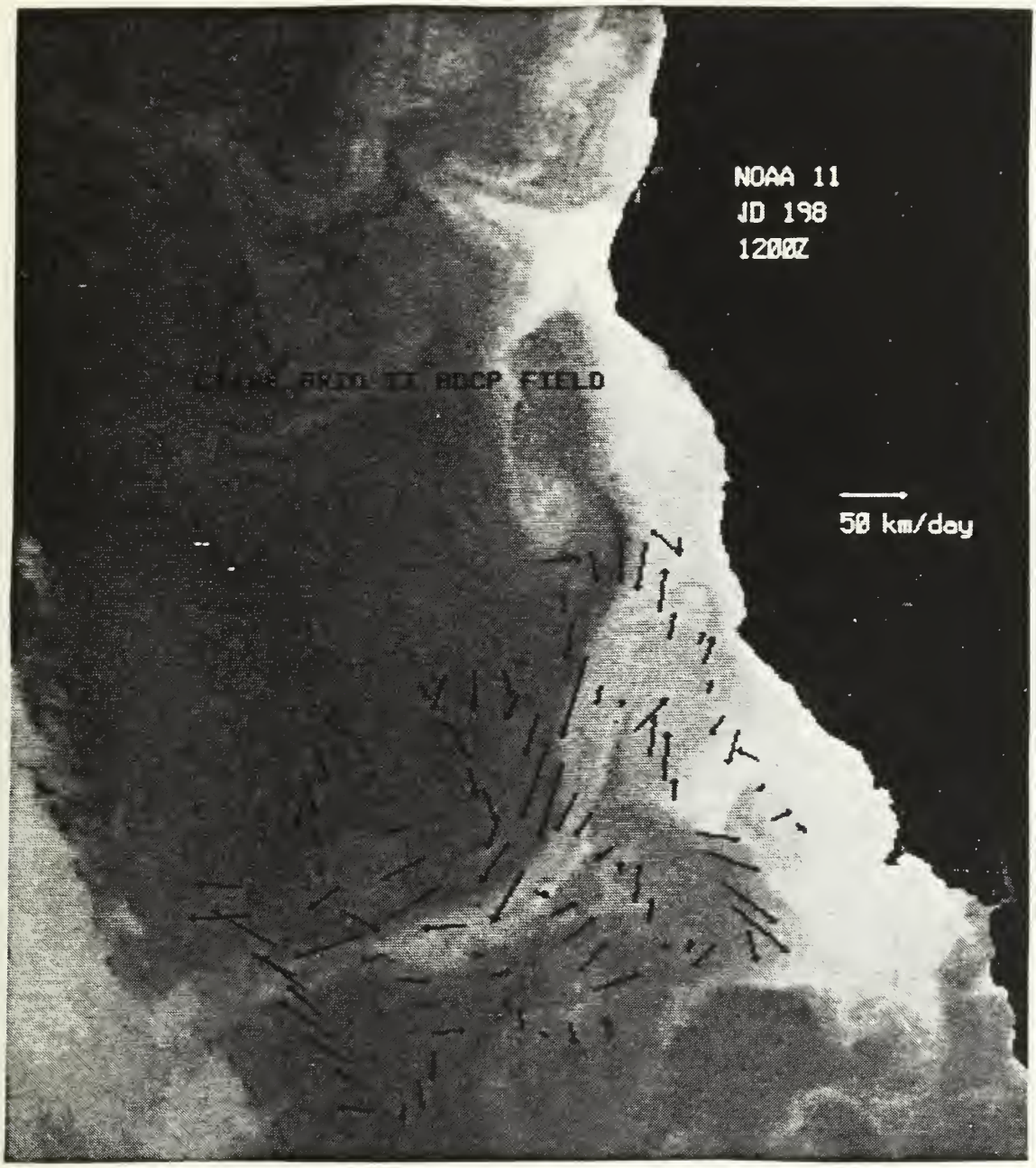

Fig. 6. CTZ88 Grid II ADCP Field on Image 19812: Line A is to the northwest proceeding to G in the southwest

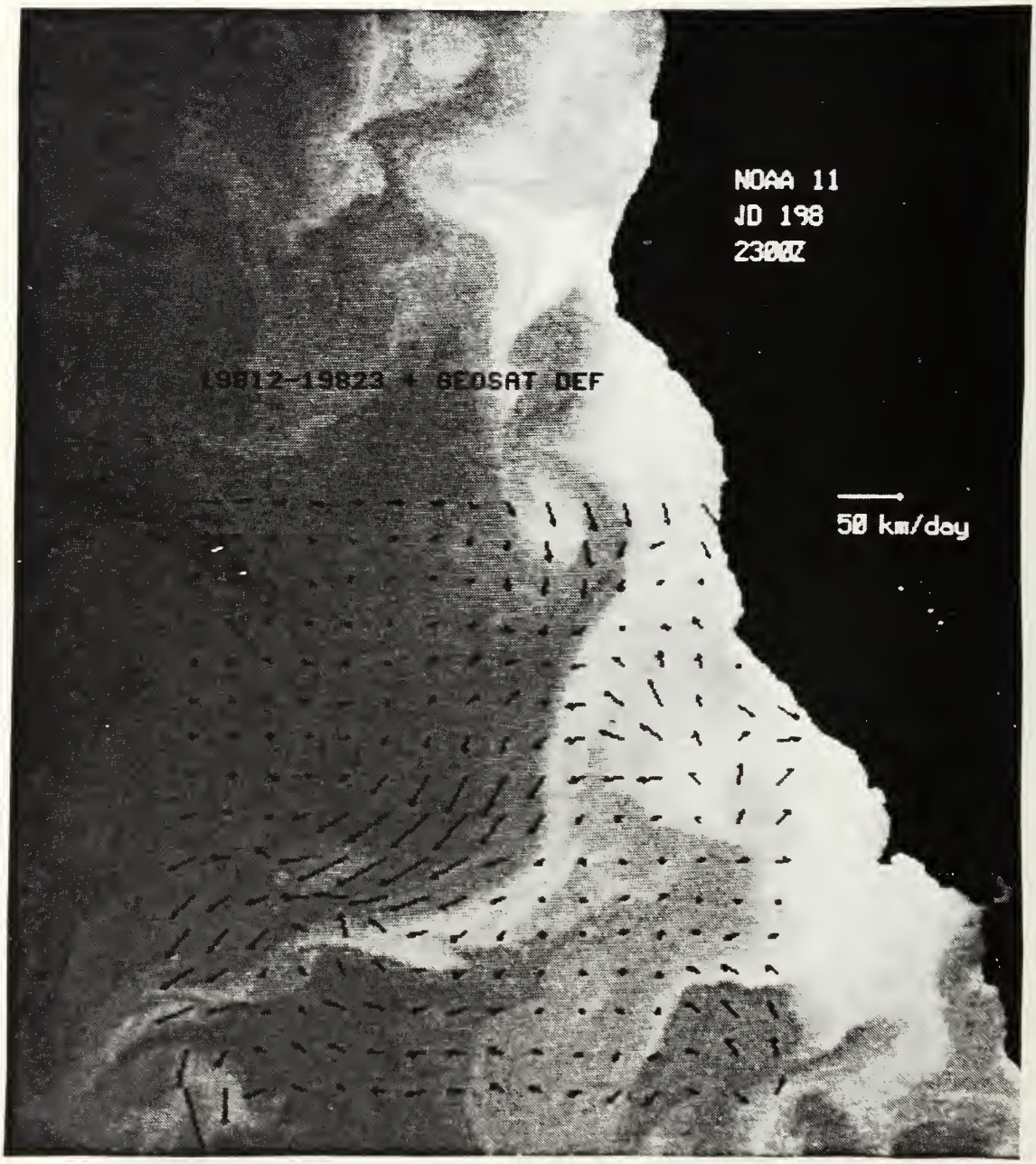

Fig. 7. 19812-19823 Inversion-alone solution on Image 19823

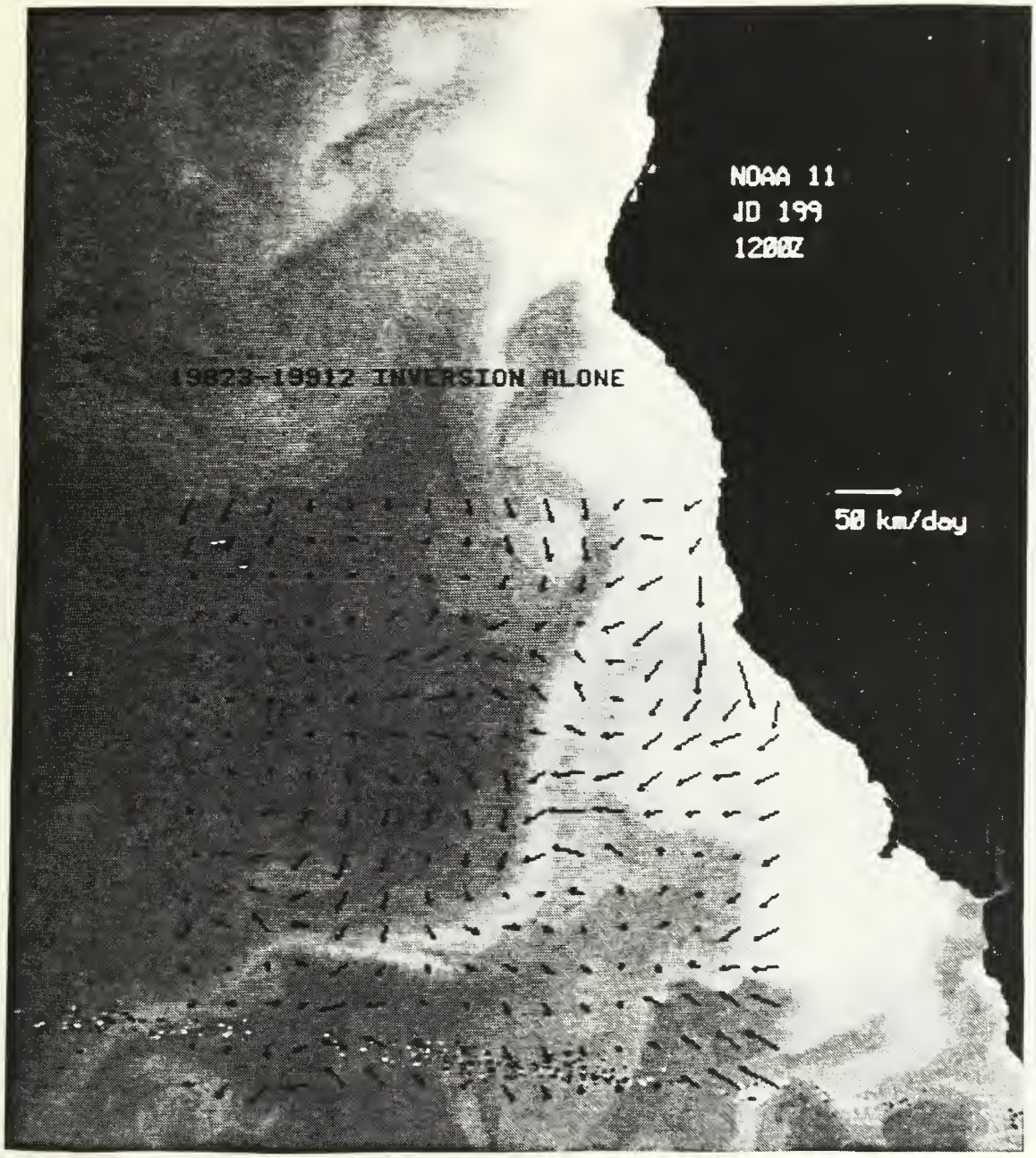

Fig. 8. 19823-19912 Inversion-alone solution on Image 19912

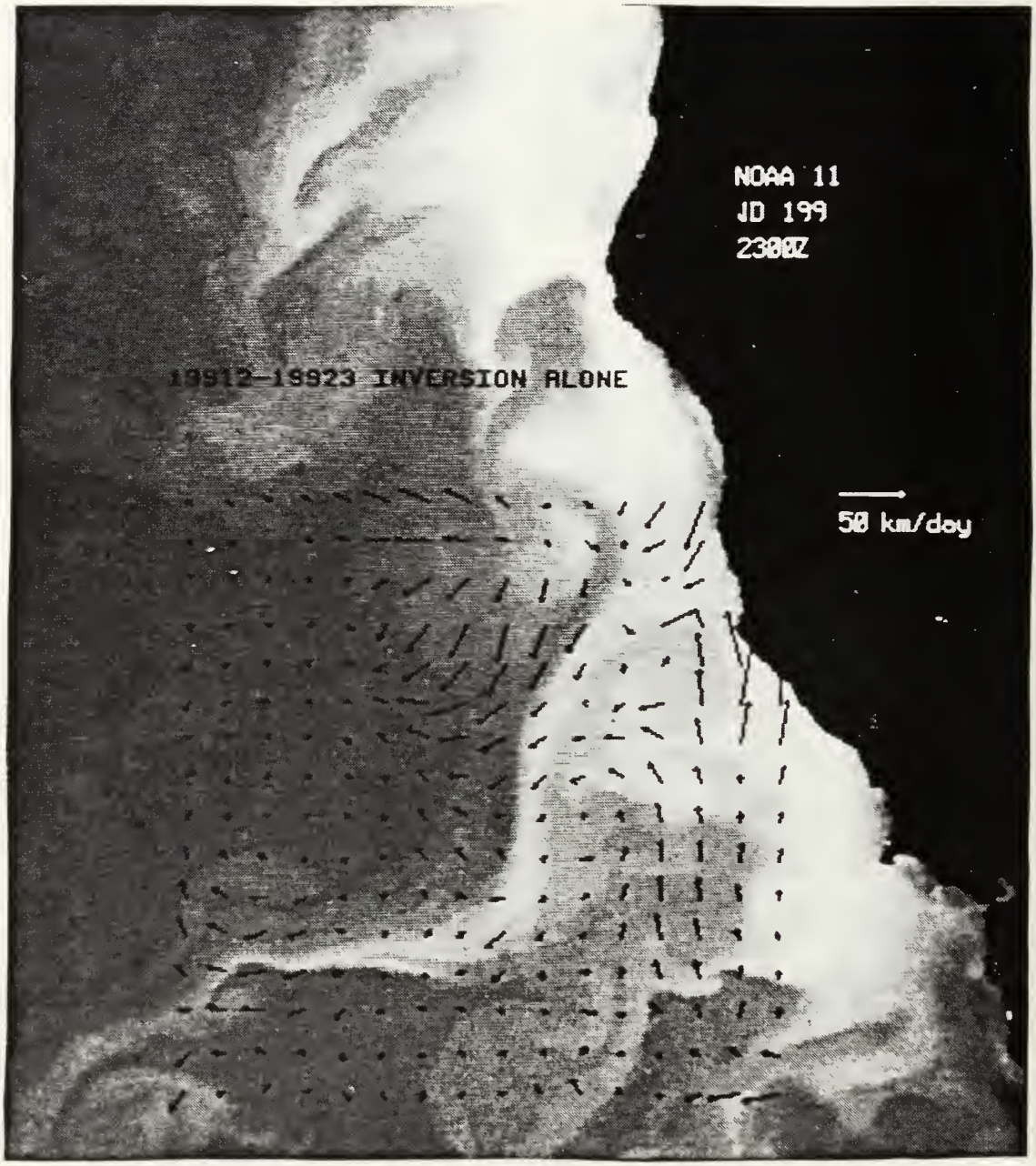

Fig. 9. 19912-19923 Inversion-alone solution on Image 19923

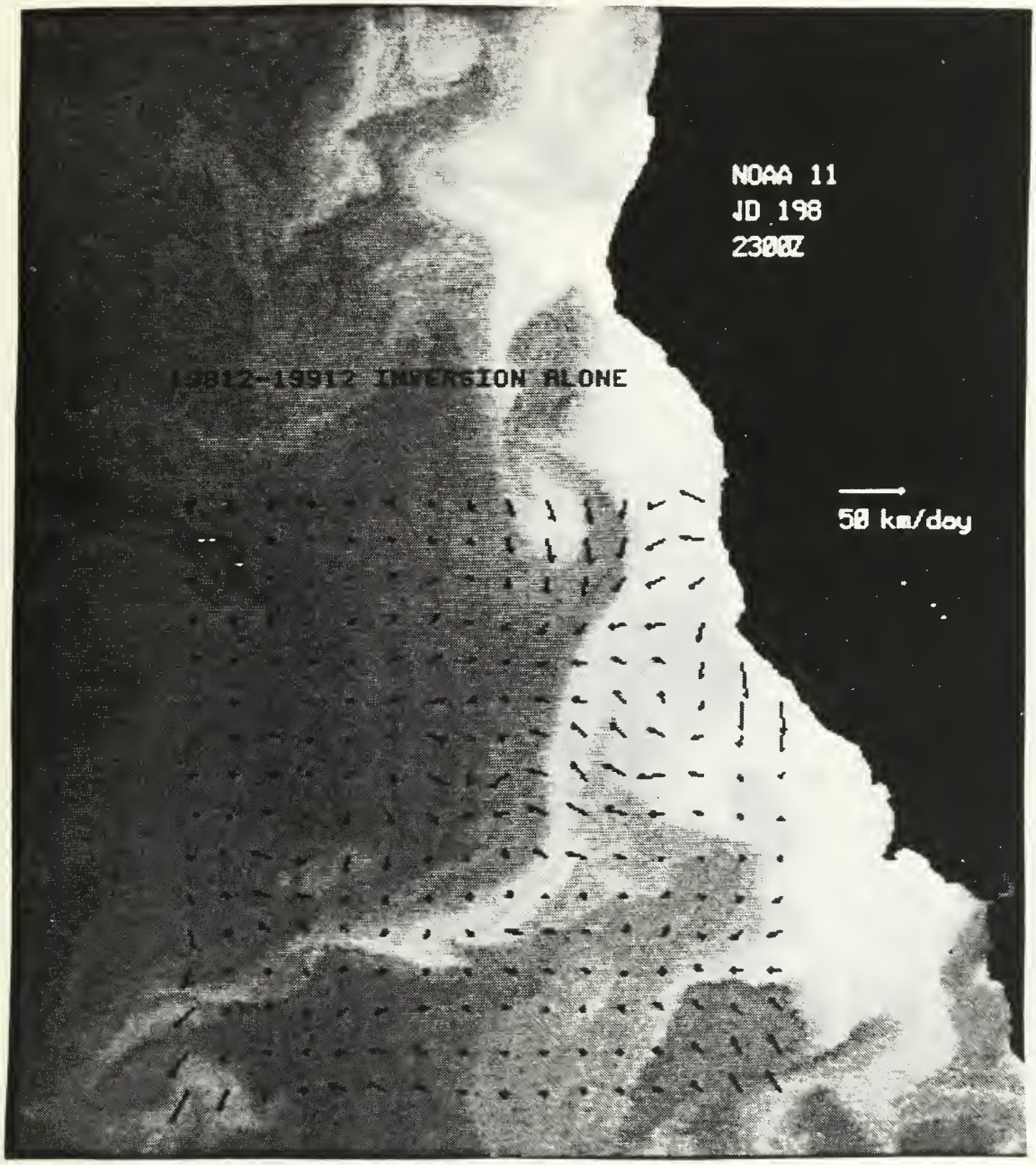

Fig. 10. 19812-19912 Inversion-alone solution on Image 19823

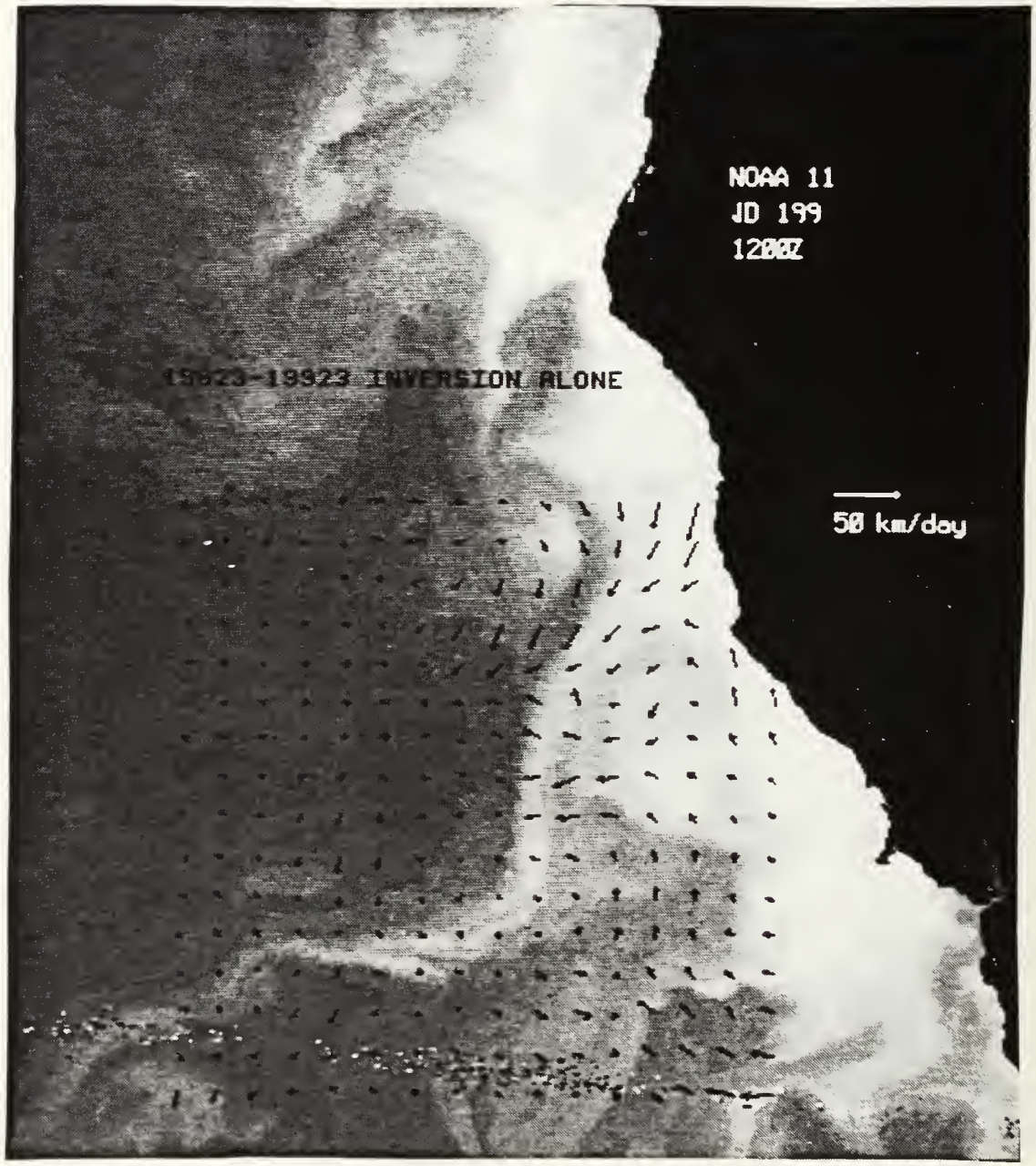

Fig. 11. 19823-19923 Inversion-alone solution on Image 19912

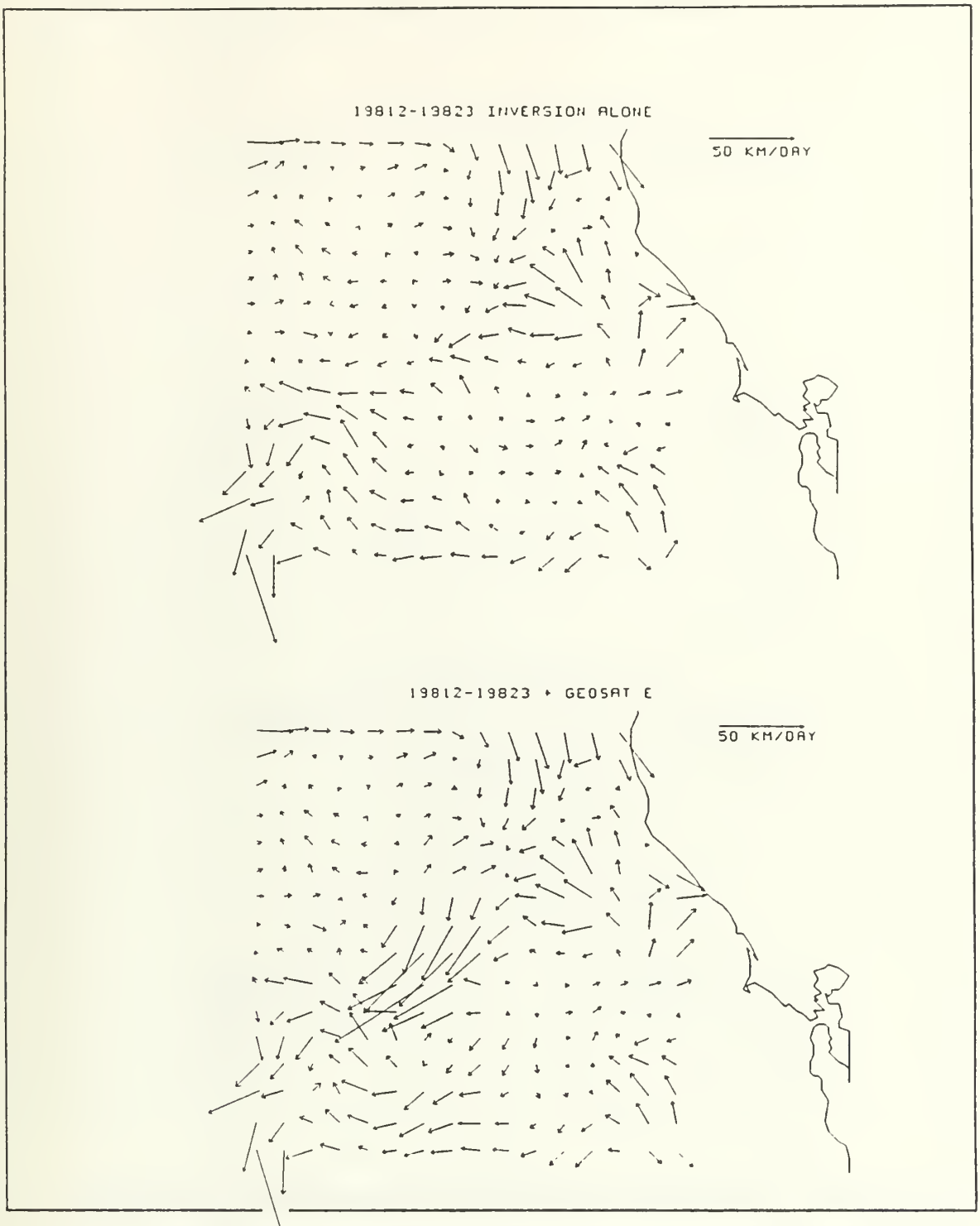

Fig. 12. 19812-19823 Solution with data line E added: The inversion-alone solution for the image pair is repeated as the top figure

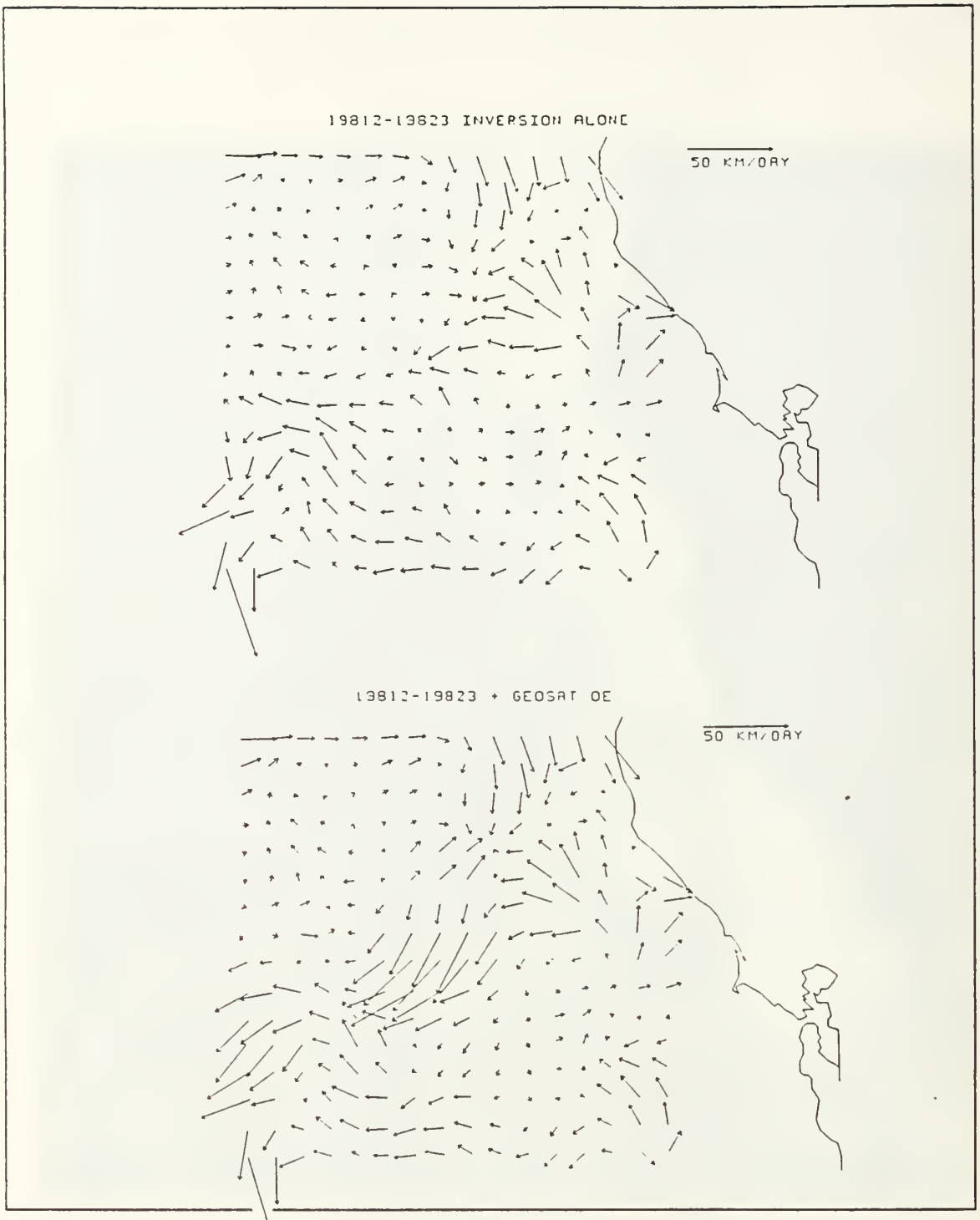

Fig. 13. 19812-19823 Solution with data lines DE added

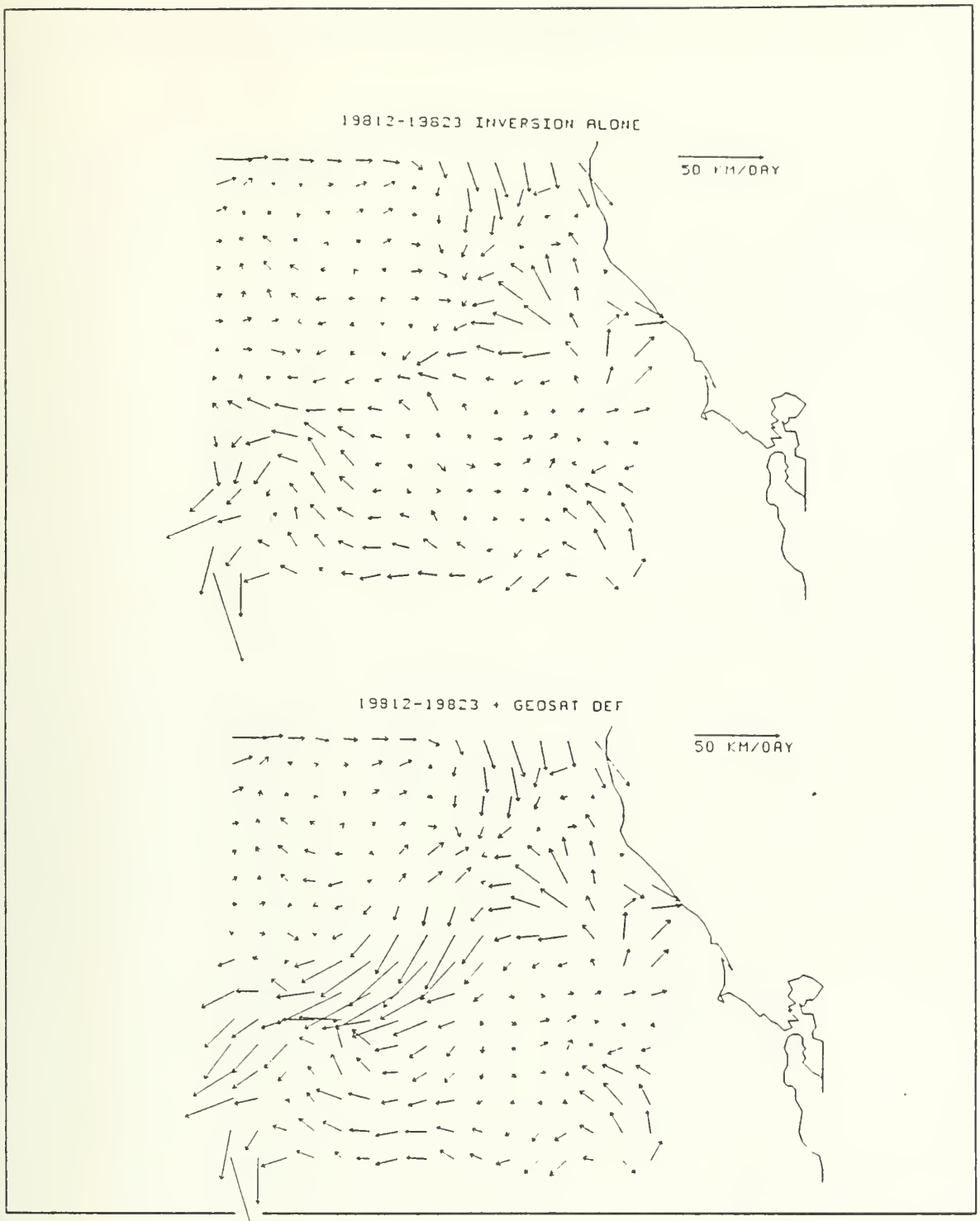

Fig. 14. 19812-19823 Solution with data lines DEF added

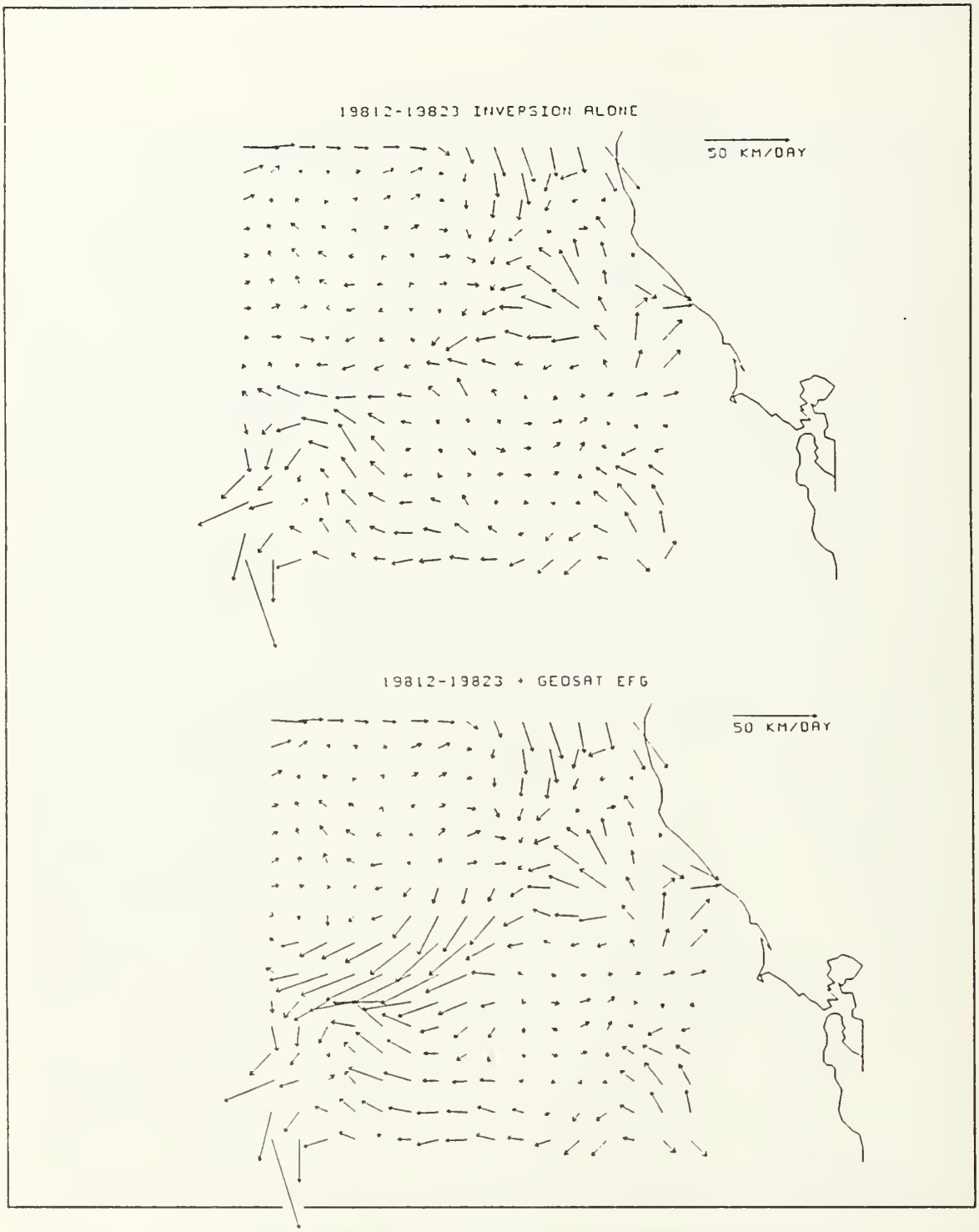

Fig. 15. 19812-19823 Solution with data lines EFG added

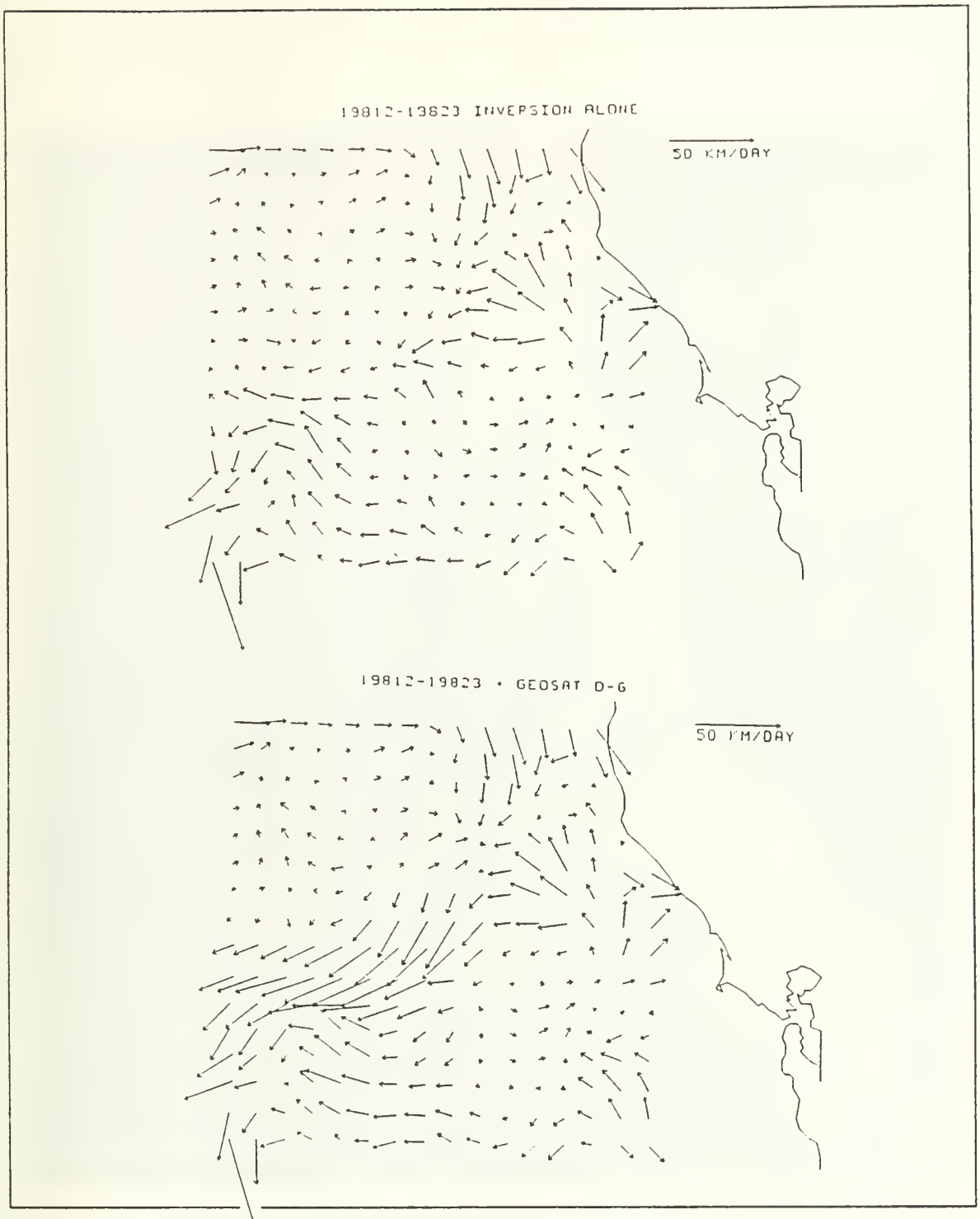

Fig. 16. 19812-19823 Solution with data lines D-G added

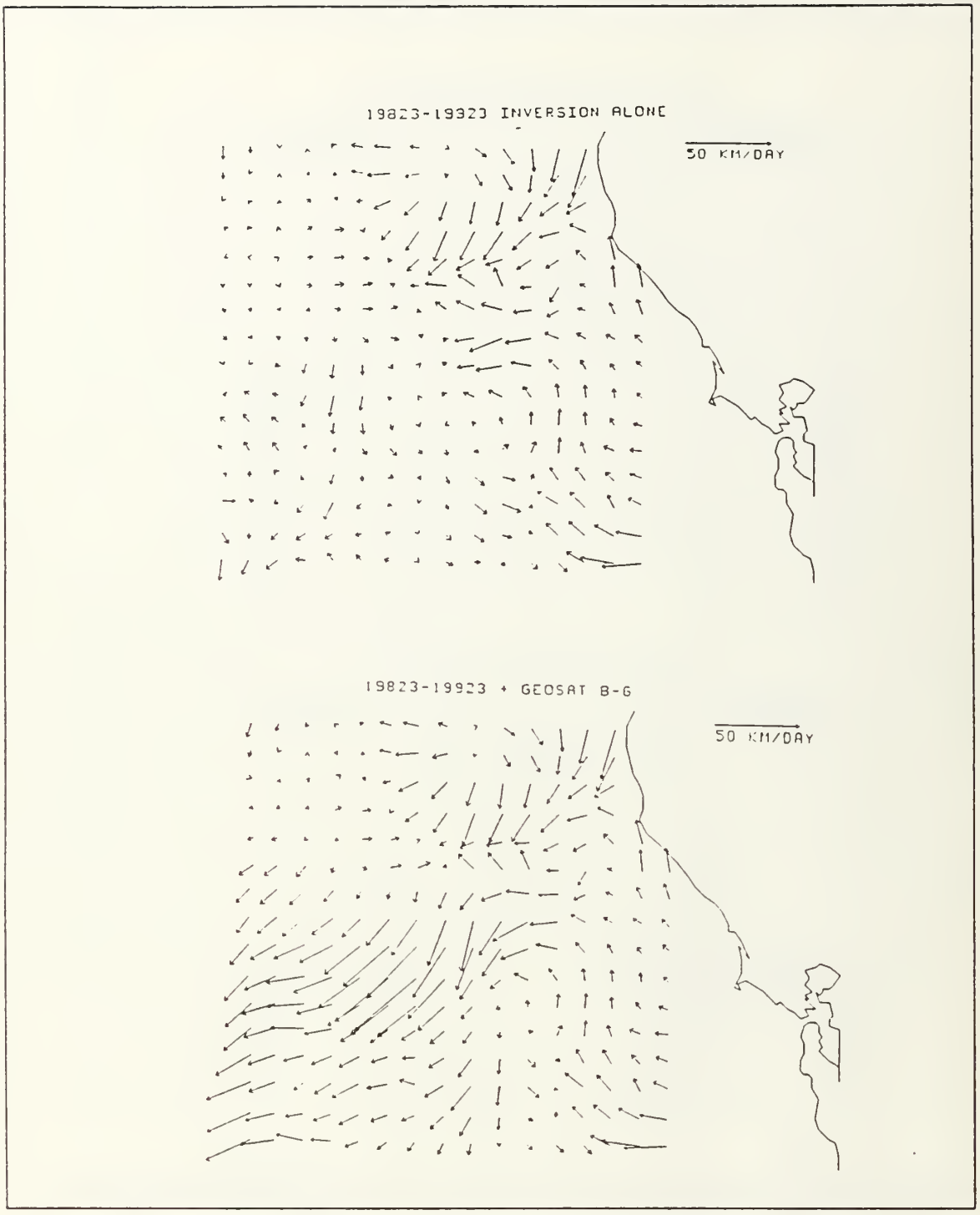

Fig. 17. 19823-19923 Solution with all velocity data added

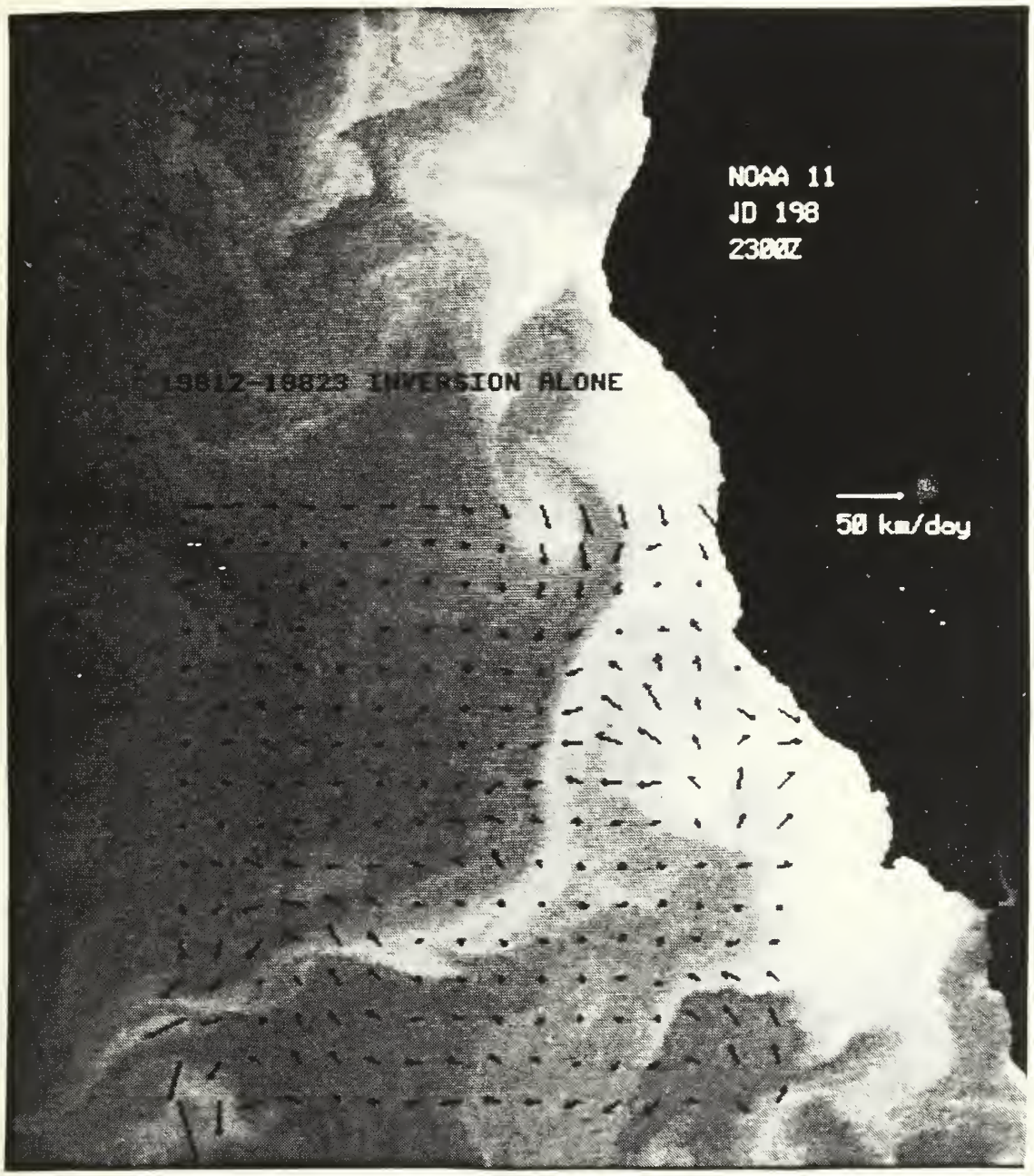

Fig. 18. 19812-19823 plus DEF data lines on Image 19823

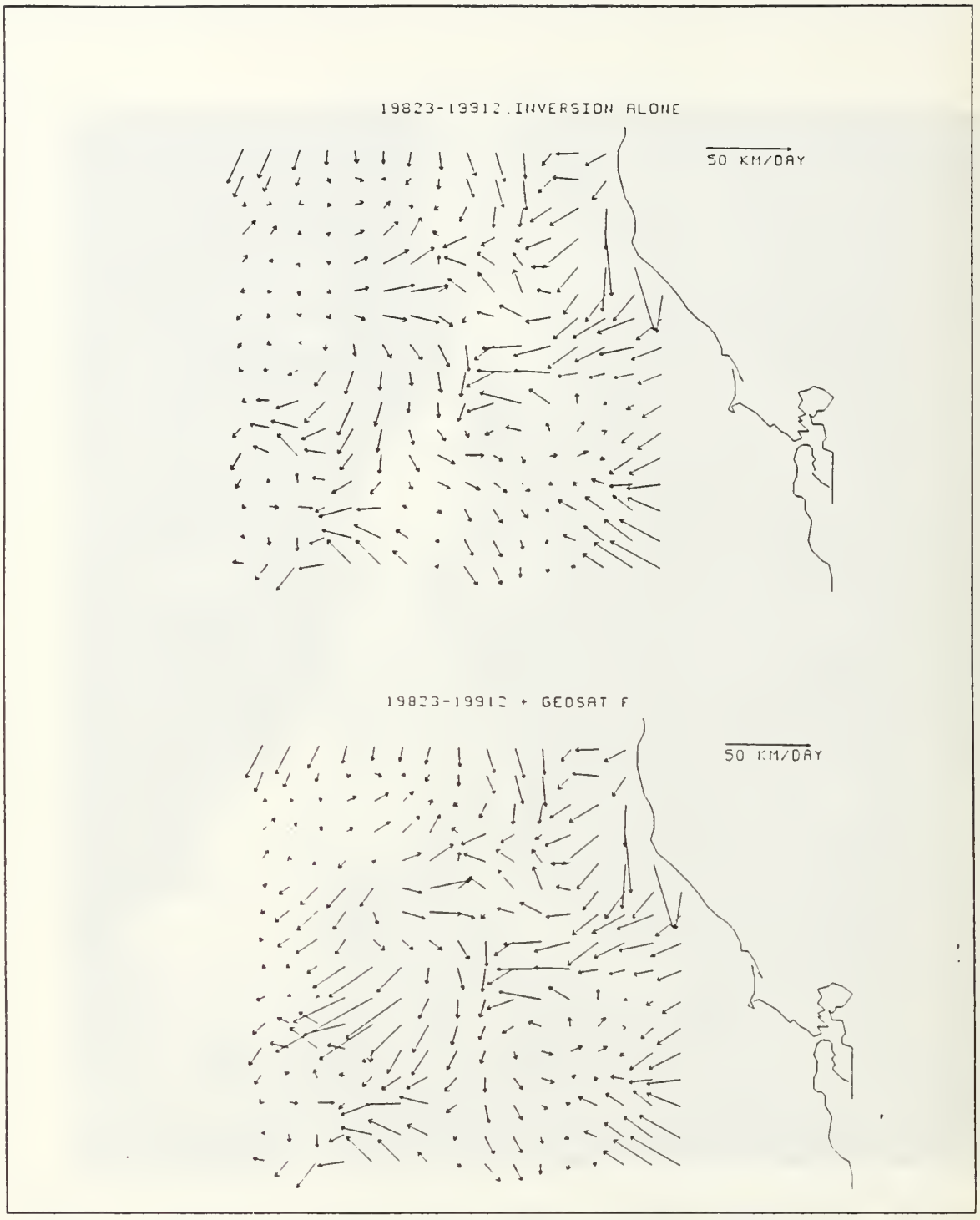

Fig. 19. 19823-19912 Solution with data line E added

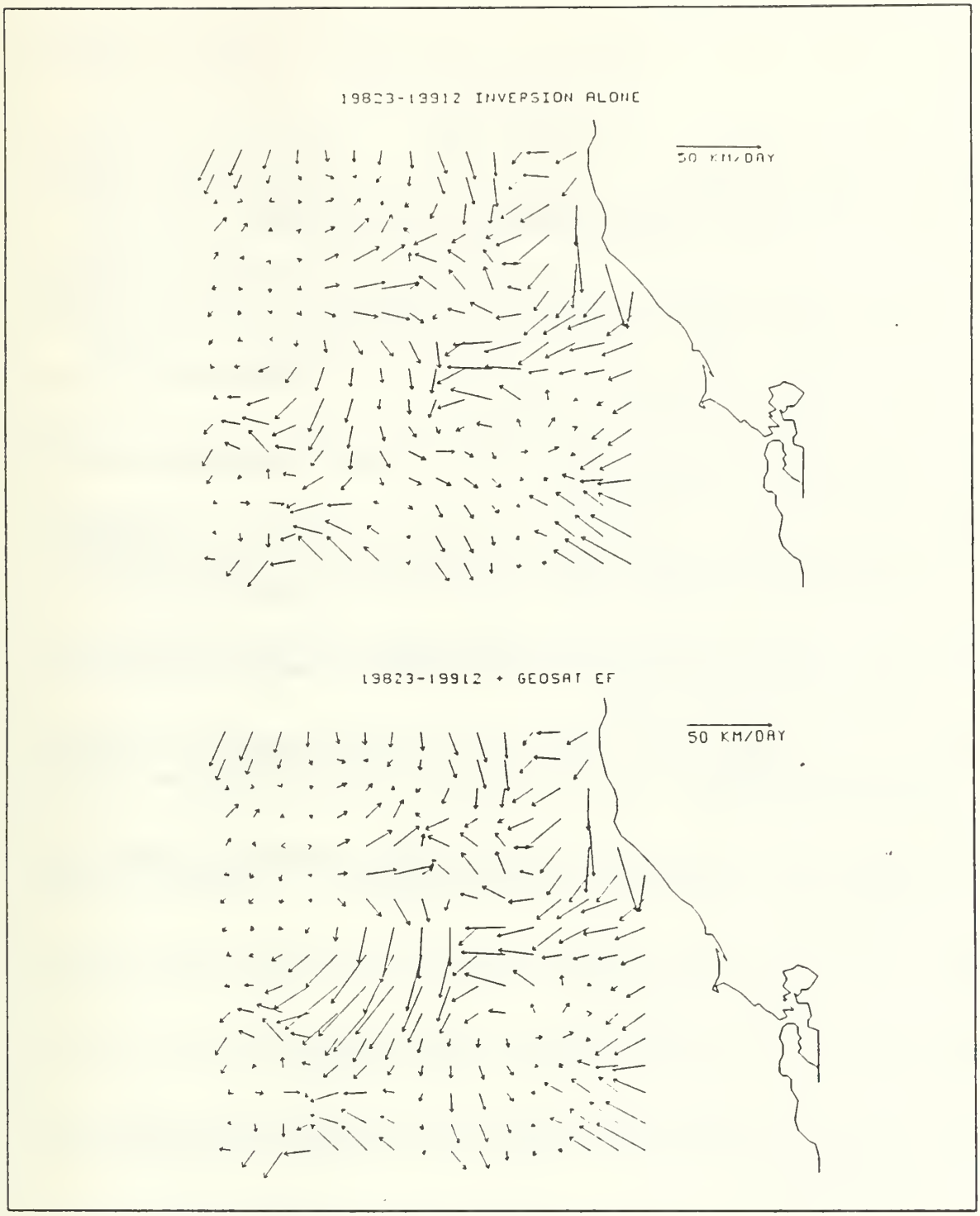

Fig. 20. 19823-19912 Solution with data lines EF added

REFERENCES

Cheney, R.E., B.C. Douglas, R.W. Agreen, L. Miller, D.L. Porter, and N.S. Doyle, 1987: Geosat altimeter geophysical data record user handbook, *NOAA Tech. Memo. NOS NGS-46*, Natl. Ocean. Serv., Rockville, Md., 29 pp.

Emery, W.J., A.C. Thomas, and M.J. Collins, 1986: An objective method for computing advective surface velocities from sequential infrared satellite images, *J. Geophy. Res.*, **86**, 12,865-12,878.

Fiadeiro, M.E., and G. Veronis, 1982: On the determination of absolute velocities in the ocean. *J. Mar. Res.*, **40**(Suppl.), 159-182.

Fiadeiro, M.E., and G. Veronis, 1984: Obtaining velocities from tracer distributions. *J. Phys. Oceanogr.*, **14**, 1734-1746.

Huyer, A., P.M. Kosro, J. Fleischbein, S.R. Ramp, T. Stanton, L. Washburn, R. Chavez, and T. Cowles, Currents and water masses of the Coastal Transition Zone off Northern California, June to August 1988, *J. Geophys. Res.*, in press.

Joyce, T.M., C. Wunsch, and S.D. Pierce, 1986: Synoptic Gulf Stream velocity profiles through simultaneous inversion of hydrographic and acoustic doppler data. *J. Geophys. Res.*, **91**, 7573-7585.

Leese, J.A., C.S. Novak, and B.B. Clarke, 1971: An automated technique for obtaining cloud motion from geosynchronous satellite data using cross correlation. *J. Appl. Meteorol.*, **10**, 110-132.

McClain, E.P., W.G. Pichel, and C.C. Walton, 1985: Comparative performance of AVHRR-based multichannel sea surface temperatures. *J. Geophys. Res.*, **90**, 11,587-11,601.

Kelly, K.A., 1989: An inverse model for near-surface velocity from infrared images. *J. Phys. Oceanogr.*, **19**, 1845-1864.

Kelly, K.A. and S.T. Gille, 1990: Gulf Stream surface transport and statistics at 69°W from the Geosat altimeter. *J. Geophys. Res.*, **95**, 3149-3161.

Kosro, P.M., 1985: Shipboard acoustic current profiling during the Coastal Ocean Dynamics Experiment. Ph.D. thesis, Scripps Inst. of Oceanogr., La Jolla, Calif., SIO Ref. 85-8, 119 pp.

Roemmich, D., 1979: The application of inverse methods to problems in ocean circulation. Ph.D. thesis, Massachusetts Institute of Technology/Woods Hole Oceanographic Institution WHOI 80-6, 193 pp.

Roemmich, D., 1981: Circulation of the Caribbean Sea: A well-resolved inverse problem. *J. Geophy. Res.*, *86*, 7993-8005.

Roemmich, D. and C. Wunsch, 1982: On combining satellite altimetry with hydrographic data. *J. Mar. Res.*, **40**(Suppl.), 605-619.

Stewart, R.H., 1985: *Methods of Satellite Oceanography.* Los Angeles: University of California Press, 360 pp.

Svejkosky, S., 1988: Sea surface flow estimation from Advanced Very High Resolution Radiometer and Coastal Zone Color Scanner satellite imagery: A verification study. *J. Geophys. Res.*, **93**, 6735-6743.

Tokmakian, R., P.T. Strub, and J. McClean-Padman, Objective estimation of surface velocities from sequential IR images, part 2: RMS error as determined from model simulation and application to AVHRR and CZCS imagery, unpublished manuscript, submitted to *J. Atmos. Oceanic Tech.*

Wunsch, C., 1978: The North Atlantic general circulation west of 50W determined by inverse methods. *Rev. of Geophys. and Space Phys.*, **16**, 583-620.

Wunsch, C., 1985: Can a tracer field be inverted for velocity? *J. Phys. Oceanogr.*, **15**, 1521-1531.

INITIAL DISTRIBUTION LIST

		No. Copies
1.	Defense Technical Information Center Cameron Station Alexandria, VA 22304-6145	2
2.	Library, Code 52 Naval Postgraduate School Monterey, CA 93943-5002	2
3.	Chairman (Code OC) Department of Oceanography Naval Postgraduate School Monterey. CA 93943-5000	1
4.	Assistant Professor Steven R. Ramp (Code OC/Ra) Department of Oceanography Naval Postgraduate School Monterey, CA 93943-5000	2
5.	Adjunct Research Professor Newell Garfield (Code OC/Gf) Department of Oceanography Naval Postgraduate School Monterey, CA 93943-5000	2
6.	Commanding Officer Oceanographic Unit Four FPO San Francisco, CA 96662-7104	1
7.	Commanding Officer Naval Oceanographic Office Stennis Space Center, MS 39522-5001	1
8.	Commanding Officer Naval Oceanic and Atmospheric Research Laboratory Stennis Space Center, MS 39529-5004	1
9.	Dr. Kathryn A. Kelly Woods Hole Oceanographic Institution Woods Hole, MA 02543	1
10.	Dr. P. Ted Strub College of Oceanography Oregon State University Corvallis, OR 97331	1

11. Dr. Tom Kinder 1
Office of Naval Research, Code 1122CS
800 N. Quincy St.
Arlington, VA 22217

12. CAPT Donald J. Taggart 1
6401 Eastleigh Ct.
Springfield, VA 22152

13. Mr. Samuel D. Gardner 1
Los Alamos National Laboratory
Mail Stop: J562
Los Alamos, NM 87545

Thesis
T122 Taggart
c.1 Determination of near-surface velocity fields in the CTZ using combined altimetric and inverse modelling techni-ques.